Electron dynamics on the surface of a three-dimensional topological insulator

Simon Loftager
Supervisor: Jens Paaske

5th of August 2012

ABSTRACT

In topological insulators momentum and spin lock in a well-defined way. With offset in this spin–momentum locking mechanism eigenenergies for Landau levels are investigated. In particular, the Landau-level eigenenergies with the warping effect included are numerically computed. The density of states for the topological surface-state electrons with and without the warping effect is found and compared. It is seen that the warping effect decreases the density of states, and that Landau levels are clearly seen in the density of states. The total density of states for the topological surface-state electrons and the bulk conduction band-induced surface-state electrons is also found numerically.

By semiclassical considerations, it is found that as the energy spectrum of Dirac electrons becomes gapped, the magnitude of Berry's phase is reduced from the non-gapped value of π to 0 as the gap strength becomes very large. Including warping has the effect of increasing the magnitude of Berry's phase. The connection between Berry's phase and the anomalous velocity is discussed and the associated anomalous quantum Hall conductivity is found to be quantized in units of $(e^2/\hbar)/(4\pi)$. Finally, the Bohr–Sommerfeld quantization condition is utilized to obtain the energies of the surface-state electrons and these energies are compared to energies computed in a finite-size Hilbert space approximation.

RESUMÉ

I topologiske insolatorer låser impulsen og spinnet på en veldefineret måde. Med afsæt i denne spin–impuls-låsningsmekanisme undersøges egenenergierne for Landau-niveauerne. I særdeleshed findes egenenergierne med warping-effekten numerisk. Tilstandstætheden for de topologiske overfladetilstandselektroner med og uden warping-effekten udregnes og sammenlignes. Man finder, at warping-effekten mindsker tilstandstætheden samt at Landau-niveauerne tydelig observeres i tilstandstætheden. Den totale tilstandstæthed for de topologiske overfladetilstandselektroner og de af bulk-ledningsbåndet inducerede overfladetilstandselektroner er også fundet numerisk.

Vha. semiklassiske betragtninger, findes det, at når der i energispektret for Dirac-elektroner åbnes et båndgab, reduceres Berrys fase fra værdien uden gab på π, til 0, når båndgabet bliver meget stort. Når warping medtages forøges størrelsen af Berrys fase. Forbindelsen mellem Berrys fase og den anomale hastighed diskuteres og den tilhørende anomale kvante-Hall-konduktivitet udregnes til at være kvantiseret i enheder af $(e^2/\hbar)/(4\pi)$. Endeligt benyttes Bohr–Sommerfelds kvanteringsbetingelse til at finde energierne for overfladetilstandselektronerne, og disse energier sammenlignes med energier udregnet med en model, hvori Hilbert-rummet approksimeres til at være endeligt.

Preface

Development of spintronics has revived research in the theory of spin–orbit coupling in metals and semiconductors. One of the main goal of spintronics is to enable manipulation of the spin of carriers by adjusting an external magnetic field, so that a spin current can be induce in the system. A good candidate for this application is a topological insulator in which surface states exhibits strong spin–orbit coupling [1].

In today's scientific literature topological insulators are often discussed together with graphene. Although the underlying physics of graphene and topological insulators is different, the physics of low-energy electrons residing in graphene has interesting parallels to the electrons at the surface of topological insulators. Hence understanding various effects of topological insulators might help us understand similar effects of graphene.

Another thing that justifies research in topological insulators is the fact that there might exist Majorana fermion states at the interface between a topological insulator and an ordinary superconductor. The existence of these Majorana fermion states is of crucial importance for the realization of quantum computation.

I would like to thank my supervisor Jens Paaske for guiding me in the making of this thesis which has been conducted at the Niels Bohr Institute in the academic year 2011/2012. I would also like to thank Logi Arnarson and Michael Bjerngaard for useful discussions.

Contents

1 Introduction

1.1 An introduction to topological insulators

1.1.1 Ordinary and topological insulators

The man-in-the-street definition of topological insulators is that they act as insulators inside the material, but are nevertheless able to conduct an electrical current on the surface of the material. This is of course merely a phenomenological definition, which does not explain the mechanisms by which this class of insulators work.

Beginning in the other end, the simplest ordinary insulator is an atom where electrons are bound in closed shells and cannot move. Band-theoretically, an insulator is defined as a band structure having its occupied valence-band states and its empty conduction-band states separated by an energy gap. Hence in a ordinary insulator, no states exist in the energy gap. This is different for a topological insulator where the strong spin–orbit interaction of the relatively heavy atoms together with time-reversal symmetry guarantees the existence of topologically protected surface states in the bulk energy gap. Going a step deeper, the difference in the ordinary and topological insulator is in the so-called topological invariant, which will be briefly reviewed later on. But let us first see what actually generates the aforementioned surface states in the topological insulators [2].

1.1.2 Origin of Rashba effect: Band inversion due to strong spin–orbit coupling

Compounds containing heavy elements, will in general display strong spin–orbit interaction. The spin–orbit effect arises when one transforms from rest frame of the atomic nucleus to the rest frame of the electron. The charged nucleus will then be seen as orbiting around the electron, resembling a current in a circular wire and this current will induce a magnetic field. This spin–orbit-induced magnetic field is given by

$$\mathbf{B}_{\mathrm{SO}} = \frac{\gamma}{c^2}\mathbf{v} \times \mathbf{E}, \tag{1.1}$$

where γ is the Lorentz factor, and

$$\mathbf{E} = -\boldsymbol{\nabla} V, \tag{1.2}$$

where V is the potential of the atomic nucleus in the material. Writing the momentum as

$$\mathbf{v} = \frac{\mathbf{p}}{m} = \frac{\hbar}{m}\mathbf{k}, \tag{1.3}$$

the spin–orbit field is

$$\mathbf{B}_{\mathrm{SO}} = -\frac{\gamma}{c^2}\frac{\hbar}{m}\mathbf{k} \times \boldsymbol{\nabla} V. \tag{1.4}$$

Now, the spin–orbit Hamiltonian is

$$H_{\mathrm{SO}} = \frac{\mu_{\mathrm{B}}}{2} g \boldsymbol{\tau} \cdot \mathbf{B}_{\mathrm{SO}}, \tag{1.5}$$

so with $\mu_{\mathrm{B}} = {}^{e\hbar}/_{2m}$, we get

$$H_{\mathrm{SO}} = \gamma g \frac{\hbar^2}{4m^2c^2}\boldsymbol{\tau} \cdot (\mathbf{k} \times \boldsymbol{\nabla} V). \tag{1.6}$$

The Rashba effect stems from breaking of inversion symmetry at the surface of the material, where the confining potential is perpendicular to the surface,

$$\boldsymbol{\nabla} V = \frac{\mathrm{d}V}{\mathrm{d}z}\hat{\mathbf{z}}. \tag{1.7}$$

The resulting Hamiltonian is there

$$H_{\mathrm{SO}} = \gamma g \frac{\hbar^2}{4m^2c^2} \frac{\mathrm{d}V}{\mathrm{d}z} \boldsymbol{\tau} \cdot (\mathbf{k} \times \hat{\mathbf{z}}). \tag{1.8}$$

With the potential in Eq. (1.7) the spin–orbit field is seen to be perpendicular to the velocity as seen in Fig. 1.1.

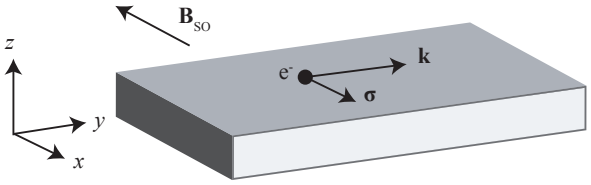

Figure 1.1: Conceptual sketch of the directions of vector fields in connection with the motion of a Dirac electron residing on the surface of a topological insulator.

If the the spin–orbit coupling in a material is strong enough it can cause the atomic orbitals to cross. For instance, in the topological insulator Bi_2Se_3, it is the two atomic orbitals, $1p_z^+$ and $2p_z^-$, that cross each other upon turning on the spin–orbit coupling, so that $2p_z^-$ has a higher energy than $1p_z^+$ after the inversion has taken place. Here $\pm$ signifies the parity of the orbital at the Γ point. This is illustrated in Fig. 1.2: First (I) bismuth orbitals hybridize with selenium orbitals, which breaks orbital degeneracy, then (II) bonding and antibonding states are formed due to inversion symmetry, then (III) due to the crystal field, the ion lattice breaks rotational symmetry, and the orbitals are further split, and finally (IV) the spin–orbit coupling breaks spin-degeneracy, but in this case with a *negative* spin–orbit-induced 'gap'. This band inversion mechanism leads to the crossing of energy bands which is the origin of the topologically protected edge states in two dimensions and surface states in three dimensions [3].

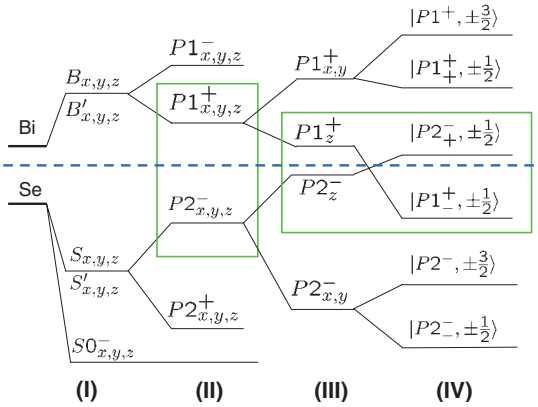

Figure 1.2: Origin of the band structure of Bi_2Se_3. The orbitals split from (I) the hybridization of Bi orbitals with Se orbitals, (II) the bonding and antibonding states due to inversion symmetry, (III) crystal field splitting, (IV) the spin–orbit coupling. From [3].

Unlike other quantum states which are characterized by a spontaneous symmetry breaking, e.g. spontaneous translational breaking in crystals, the band inversion transition is not characterized by any spontaneous symmetry breaking, but rather by a *topological phase transition*: The fundamental symmetry of the lattice is the same on either side of the transition, but there is a change in the topological invariant ν_0 of the ground state. Without getting lost in mathematical topology we will briefly summarize the most important features of the topological part of topological insulators. But first we shall describe how the k-space landscape of a topological insulator looks like.

In the surface Brillouin zone of a topological insulator there are four time-reversal invariant points (TRIM) Γ_1, Γ_2, Γ_3 and Γ_4, as illustrated in Fig. 1.4. Due to Kramers' theorem, which states that all eigenstates of a time-reversal invariant Hamiltonian are at least twofold degenerate, the surface states are doubly degenerate at these TRIM points. In topological insulators the crossing of the valence band with the conduction band is centered at such a TRIM point. Due to the resemblance of this conical, low-energy band structure at the TRIM points to the Dirac-like light cone of a relativistic system, these crossing points are also called *Dirac points*. The fact that the Dirac point is centered at

a TRIM point guarantees the robustness of the Dirac spectrum against weak time-reversal invariant perturbations [2].

In the gap of the bulk-valence and bulk-conduction band topologically protected surface states. Here topologically protected means that the electronic bands of these surface states cannot be separated—i.e. no formation of an *surface* energy gap—by a continuously smooth perturbation, such as an external electrical field. This being said, it is important to realize that the time-reversal symmetry must not be broken, which it is e.g. by a magnetic field or by ordered magnetic impurities. An example of the robustness of the topological surface states is the suppression of backscattering of a Dirac electron on a nonmagnetic impurity: Backscattering simply means that the electron's momentum is rotated by π, but this requires the electron's spin to flip, also by π, because of the spin–momentum locking mechanism. But in order for this spin-flip process to take place, a breaking of the time-reversal symmetry is required, which nonmagnetic impurities do not provide. A short calculation supporting the above argument is given in Sec. A.1.

The surface states are said to be helical, which means that the spin and momentum of the states are coupled in a well-defined way, also referred to as spin–momentum locking. See Fig. 1.3 for the spin texture on the constant-energy contour in the low-energy regime. Here it is also indicated that opposite momenta have opposite spins. Since a state with a giving momentum $\mathbf{k}$ has a unique spin $\boldsymbol{\tau}$, these Dirac fermions have no spin degeneracy, except at the Dirac point, where the spins are doubly degenerated.

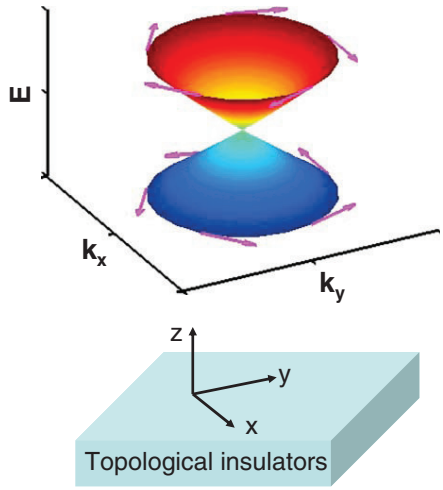

Figure 1.3: Spin texture of a topological insulator. The momentum and spin of the particles and holes are locked at right angle. For the conduction band (blue part of the cone), the helicity is left handed while for the valence band (red part of the cone), it is right handed. From [3].

Topologically, all insulators can be classified according to the four $\mathbb{Z}_2$ topological invariants ν_0, ν_1, ν_2 and ν_3. These quantities do not change under small perturbations, e.g. due to disorder, continuous geometric deformations, disorder, electron–electron interactions etc. There are two classes of topological insulators: The *weak topological insulator* and the *strong topological insulator*. As shown in Fig. 1.4, the Fermi circle in the Brillouin zone of a weak topological insulator encloses an *even* number of Dirac points (i.e. zero). This corresponds to the topological invariant $\nu_0 = 0$. For a strong topological insulator the Fermi circle in the Brillouin zone will enclose an *odd* number of Dirac points (e.g. one as in the figure) [2, 4]. In this thesis the focus will be on three-dimensional strong topological insulators, i.e. $\nu_0 = 1$, but except from this no reference to topological concepts will be made.

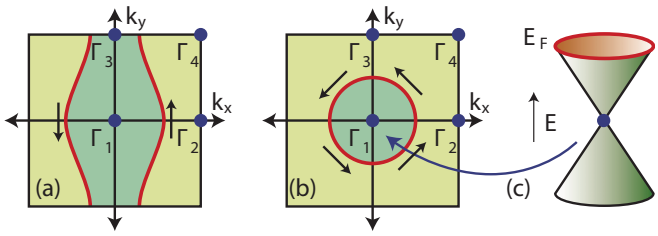

Figure 1.4: The weak topological insulator in (a) encloses an even number of Dirac points, whereas the strong topological insulator in (b) encloses an odd number of Dirac points in a 2D band structure shown in (c). From [2].

1.2 Models for topological insulators

When studying topological insulators, we will draw a distinction between the low-energy regime and an energy regime in which higher-order terms have to be included in order to describe the system correctly. To make the designation clear, electrons which reside at the Dirac point, are called Dirac electrons, and they will obey the Dirac equation. Electrons, which are higher in energy acquiring a nonlinear dispersion relation, will be called topological-insulator electrons, emphasizing that they describe the surface states of topological insulators most accurately.

1.2.1 Model Hamiltonian for the low-energy surface states

As discussed in [3] the model Hamiltonian for a topological insulator can be found either from symmetry principles, the theory of invariants or by the $\mathbf{k}\cdot\mathbf{p}$ method. [3] showed that the surface states of Dirac electrons are well-described by the Rashba Hamiltonian,

$$H_{\mathrm{R}} = \hbar v_{\mathrm{F}}(\boldsymbol{\tau}\times\mathbf{k})\cdot\hat{\mathbf{z}}, \tag{1.9}$$

where $\mathbf{p}=\hbar\mathbf{k}=\hbar(k_x,k_y,k_z)$ is the momentum of the Dirac electron with Fermi velocity v_{F} and $\boldsymbol{\tau}$ is an array of Pauli matrices defined by

$$\boldsymbol{\tau}\equiv(\tau_x,\tau_y,\tau_z). \tag{1.10}$$

From Eq. (1.9) we see the effect of the spin–momentum locking explicitly, as the spin vector and momentum vector always couple at a fixed angle, which is also illustrated in Fig. 1.1. Near the Dirac-point energy the spin vector lies solely in xy plane. By the vector identity

$$\mathbf{a}\cdot(\mathbf{b}\times\mathbf{c}) = \mathbf{b}\cdot(\mathbf{c}\times\mathbf{a}), \tag{1.11}$$

the Hamiltonian in Eq. (1.9) can be written as

$$H_{\mathrm{R}} = \hbar v_{\mathrm{F}}(\hat{\mathbf{z}}\times\boldsymbol{\tau})\cdot\mathbf{k} = \hbar v_{\mathrm{F}}(k_y\tau_x - k_x\tau_y). \tag{1.12}$$

Utilizing the Pauli matrices the above Hamiltonian becomes

$$H_{\mathrm{R}} = \hbar v_{\mathrm{F}}\begin{pmatrix}0 & k_y+\mathrm{i}k_x\\ k_y-\mathrm{i}k_x & 0\end{pmatrix} = \hbar v_{\mathrm{F}}\begin{pmatrix}0 & \mathrm{i}(k_x-\mathrm{i}k_y)\\ -\mathrm{i}(k_x+\mathrm{i}k_y) & 0\end{pmatrix}, \tag{1.13}$$

and with the ladder operators for the momentum, $k_\pm\equiv k_x\pm\mathrm{i}k_y$, we have

$$H_{\mathrm{R}} = \hbar v_{\mathrm{F}}\begin{pmatrix}0 & \mathrm{i}k_-\\ -\mathrm{i}k_+ & 0\end{pmatrix} = \hbar v_{\mathrm{F}}\begin{pmatrix}0 & \mathrm{i}k_-\\ (\mathrm{i}k_-)^* & 0\end{pmatrix}, \tag{1.14}$$

Diagonalizing the Rashba Hamiltonian yields the eigenenergies in the low-energy limit,

$$E_\pm(k) = \varepsilon_{\mathrm{D}} \pm \hbar v_{\mathrm{F}}k, \tag{1.15}$$

where the Dirac-point energy ε_{D} has been included. This merely plays the role as the chemical potential. As seen from the Eq. (1.15), there exists two eigenenergies belonging to the helicity states a Dirac electron can occupy: One state with a positive helicity, $\eta=+$, and another state with a negative helicity, $\eta=-$.

1.2.2 Model Hamiltonian with warping effect

The model described by Eq. (1.12) is de facto only the simplest nontrivial approximation to the real band structure of a topological insulator. The hexagonal crystal structure of the material will induce an anisotropy effect of the bands in momentum space, called the *warping effect*, whose strength is set by the parameter λ. This effect is very pronounced in the topological insulator Bi_2Te_3. The usual warping term is a third order perturbation in k of this crystal anisotropy.

The warping effect is introduced via the warping Hamiltonian,

$$H_{\mathrm{W}} = 2\hbar^3\lambda k_x(k_x^2-3k_y^2)\tau_z = 2\hbar^3\lambda k^3\cos 3\theta\,\tau_z. \tag{1.16}$$

The model Hamiltonian for the surface states on a three-dimensional topological insulator is

$$H = \varepsilon_{\mathrm{D}}\tau_0 + H_{\mathrm{R}} + H_{\mathrm{W}}, \tag{1.17}$$

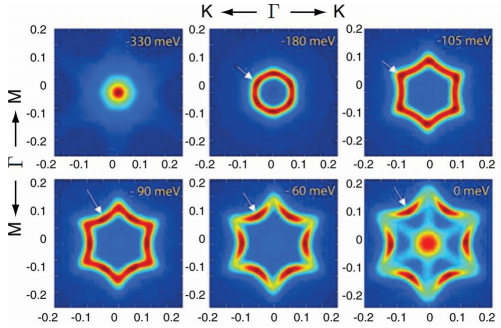

Figure 1.5: Hexagonal warping of surface states in Bi_2Te_3 probed at various energies from $E = -330$ meV to $E = 0$ meV. From [2].

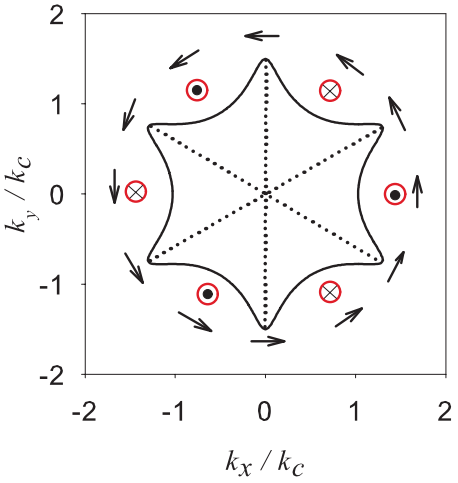

Figure 1.6: Warping effects on the spin. The spin vector of the electron obtains a finite out-of-plane component when then warping effect of Eq. (1.16) is included. From [5].

where H_{R} is the Rashba Hamiltonian in Eq. (1.12). The full Hamiltonian is therefore

$$H = \varepsilon_{\mathrm{D}}\tau_0 + \hbar v_{\mathrm{F}}(k_y\tau_x - k_x\tau_y) + 2\hbar^3\lambda k^3\cos 3\theta\,\tau_z, \tag{1.18}$$

where τ_0 denotes the identity matrix. Since $k_\pm \equiv k_x \pm \mathrm{i}k_y = k\,\mathrm{e}^{\pm\mathrm{i}\theta}$, the model Hamiltonian with warping can also be written as

$$H = \varepsilon_{\mathrm{D}}\tau_0 + \hbar v_{\mathrm{F}}(k_y\tau_x - k_x\tau_y) + \hbar^3\lambda(k_+^3 + k_-^3)\tau_z. \tag{1.19}$$

The last expression for Hamiltonian will prove useful when we investigate the effects of a magnetic field on the topological-insulator surface state. The eigenenergies of the model Hamiltonian in Eq. (1.18) gives the energy spectrum of a topological-insulator surface-state electron,

$$E_\pm(k,\theta) = \varepsilon_{\mathrm{D}} \pm \sqrt{(\hbar v_{\mathrm{F}}k)^2 + (2\hbar^3\lambda\cos 3\theta k^3)^2}, \tag{1.20}$$

or

$$E_\pm(k_x,k_y) = \varepsilon_{\mathrm{D}} \pm \sqrt{(\hbar v_{\mathrm{F}})^2(k_x^2+k_y^2) + \left(2\hbar^3\lambda k_x(k_x^2-3k_y^2)\right)^2}. \tag{1.21}$$

This energy spectrum is plotted in Fig. 1.7. A contour plot of the same energy spectrum is seen in Fig. 1.8. We note that the warping term in Eq. (1.18) is negligible for small values of k, and the Hamiltonian reduces to that in Eq. (1.12). At high energies the constant-energy contours becomes warped into a snowflake-shaped contour. As the warping effect deforms the Fermi surface, the spin vector will acquire a finite out-of-plane component as indicated in Fig. 1.6 [6].

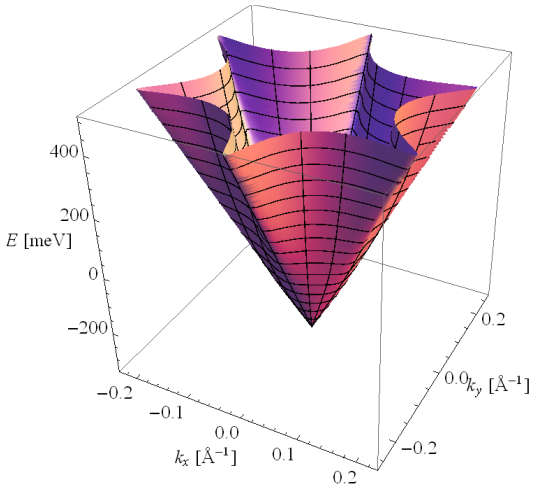

Figure 1.7: The energy spectrum Eq. (1.20) of surface-state electrons with warping effect.

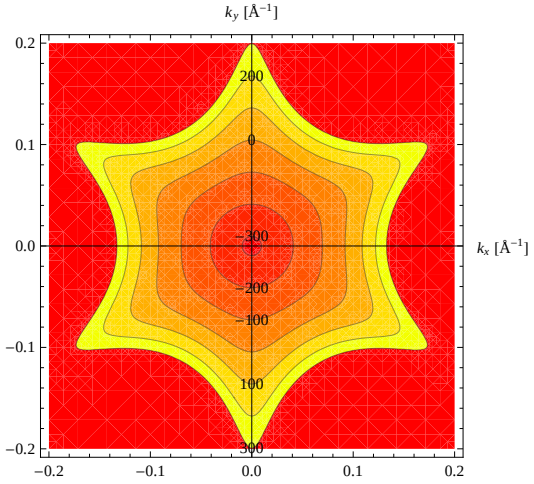

Figure 1.8: Contour plot of the energy spectrum Eq. (1.20) of surface-state electrons with warping effect. The contours are plotted from energies −300 meV up to 300 meV in steps of 100 meV.

1.3 Bismuth selenide (Bi_2Se_3)

Bismuth selenide, consisting of bismuth (Bi, atom number 83) and selenium (Se, atom number 34), is a tetradymite semiconductor which is shown to have topologically protected surface states, making it a topological insulator. Its crystal structure, shown in Fig. 1.9, is rhombohedral with quintuple layers oriented perpendicular to the trigonal c-axis, displaying threefold rotational symmetry. The covalent bonding within each quintuple layer (intralayer coupling) is much stronger than the van der Waals forces bonding neighboring layers (interlayer coupling).

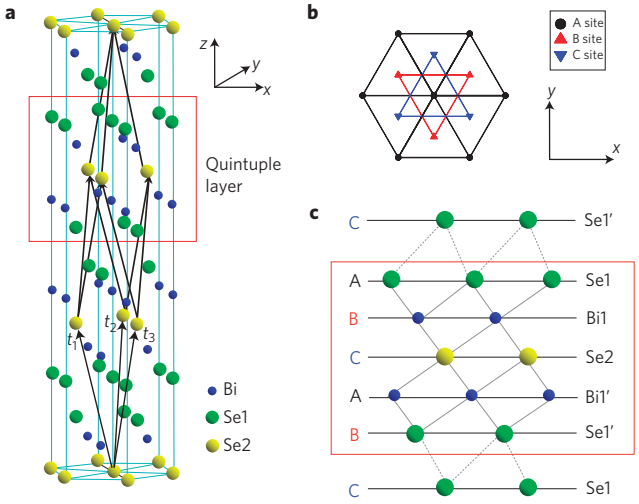

Figure 1.9: Crystal structure of Bi_2Se_3. From [7].

The bulk Brillouin zone and its projection onto the surface Brillouin zone of Bi_2Se_3 is shown in Fig. 1.10.

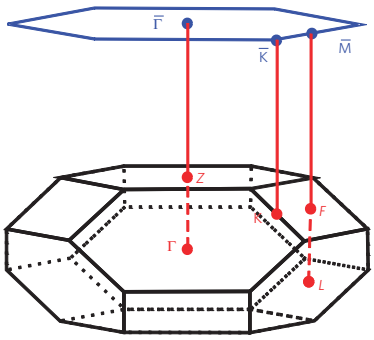

Figure 1.10: The projection of the bulk Brillouin zone (lower construction) to the surface Brillouin zone (upper construction) of Bi_2Se_3. From [7].

What makes Bi_2Se_3 special is that its surface Brillouin zone only contains a single Dirac cone, making it easier to study than other topological insulators like for instance $Bi_{1-x}Sb_x$. Bi_2Se_3 also has also gained much attention because it has a large band gap, separating the bulk valence band from the bulk conduction band by approximately 300 meV. From private communication with P. Hofmann, angle-resolved photoemission spectroscopy measurements done on Bi_2Se_3 reveal that

$$\hbar v_{\mathrm{F}} = 3100 \text{ meV Å}, \tag{1.22}$$

such that the Fermi velocity is

$$v_{\mathrm{F}} = 4.712 \cdot 10^5 \text{ m s}^{-1}, \tag{1.23}$$

and the Dirac point is located at

$$\varepsilon_{\mathrm{D}} = -330 \text{ meV}, \tag{1.24}$$

and that this material displays warping effects via a strength

$$\hbar^3 \lambda = 10^5 \text{ meV Å}^3. \tag{1.25}$$

That means that the contribution to the surface-state energy from the Dirac energy and the warping effects is of the same order, when

$$(\hbar v_{\mathrm{F}})^2 k_{\mathrm{c}}^2 = (2\lambda\hbar^3 \cos 3\theta)^2 k_{\mathrm{c}}^6, \tag{1.26}$$

so

$$k_{\mathrm{c}} = \sqrt{\frac{v_{\mathrm{F}}}{2\lambda\hbar^2 \cos 3\theta}}. \tag{1.27}$$

Choosing $2\cos 3\theta = 1$, the characteristic wavenumber is

$$k_{\mathrm{c}} \approx 0.176 \text{ Å}^{-1}, \tag{1.28}$$

which corresponds to the energy

$$E_{\mathrm{c}} = 442 \text{ meV}, \tag{1.29}$$

at which the warping can no longer be treated at a perturbation.

1.4 Zero-field density of states for surface-state electrons

Before studying the effects of applying external fields to a topologically insulating system, it is worthwhile to see how the topological surface states are distributed in these new materials. This will be the focus of this section.

1.4.1 Density of states in linear regime

The DOS per unit area per spin in a two-dimensional system with the energy spectrum

$$E_{\pm}(k) = \varepsilon_{\mathrm{D}} \pm \hbar v_{\mathrm{F}} k, \tag{1.30}$$

is given as

$$\begin{aligned} d(\varepsilon) &= \int \frac{\mathrm{d}\mathbf{k}}{(2\pi)^2} \delta\big(\varepsilon - E(k)\big) \\ &= \frac{1}{(2\pi)^2} \int_0^{2\pi} \mathrm{d}\theta \int_0^{\infty} \mathrm{d}k\, k \frac{1}{\hbar v_{\mathrm{F}}} \delta\left(k - \frac{\varepsilon - \varepsilon_{\mathrm{D}}}{\hbar v_{\mathrm{F}}}\right) \\ &= \frac{1}{2\pi(\hbar v_{\mathrm{F}})^2}(\varepsilon - \varepsilon_{\mathrm{D}}). \end{aligned} \tag{1.31}$$

So the DOS of a helical electrons near the Dirac point is linear in the energy ε and vanishes at the Dirac point.

1.4.2 Density of states with warping

Including the warping effect the energy spectrum is now given by Eq. (1.20), and the DOS probing at the energy ε is

$$\begin{aligned} d(\varepsilon) &= \int \frac{\mathrm{d}\mathbf{k}}{(2\pi)^2} \delta\big(\varepsilon - E(k)\big) \\ &= \frac{1}{(2\pi)^2} \int_0^{2\pi} \mathrm{d}\theta \int_0^{k} \mathrm{d}k\, k \sum_i \frac{\delta(k - k_i)}{|f'(k_i)|} \\ &= \frac{1}{(2\pi)^2} \sum_i \int_0^{2\pi} \mathrm{d}\theta\, \frac{k_i}{|f'(k_i)|}, \end{aligned} \tag{1.32}$$

where

$$f(k) \equiv \varepsilon - E_{\pm}(\mathbf{k}) = \varepsilon - \big(\varepsilon_{\mathrm{D}} \pm \sqrt{(\hbar v_{\mathrm{F}})^2 k^2 + (2\hbar^3 \lambda \cos 3\theta)^2 k^6}\big). \tag{1.33}$$

The k_i are determined by

$$f(k_i) = 0, \tag{1.34}$$

or

$$4\lambda^2 \hbar^6 \cos^2 3\theta k_i^6 + (\hbar v_{\mathrm{F}})^2 k_i^2 - (\varepsilon - \varepsilon_{\mathrm{D}})^2 = 0. \tag{1.35}$$

With $x \equiv k_i^2$ this equation becomes

$$(2\hbar^3 \lambda \cos 3\theta)^2 x^3 + (\hbar v_{\mathrm{F}})^2 x - (\varepsilon - \varepsilon_{\mathrm{D}})^2 = 0, \tag{1.36}$$

which has the only real solution,

$$\begin{aligned} k_i^2 = x = &\sqrt[3]{\frac{1}{2}\left(\frac{\varepsilon - \varepsilon_{\mathrm{D}}}{2\lambda\hbar^3 \cos 3\theta}\right)^2 + \sqrt{\frac{1}{27}\left(\frac{\hbar v_{\mathrm{F}}}{2\lambda\hbar^3 \cos 3\theta}\right)^6 + \frac{1}{4}\left(\frac{\varepsilon - \varepsilon_{\mathrm{D}}}{2\lambda\hbar^3 \cos 3\theta}\right)^4}} \\ &- \sqrt[3]{\left|\frac{1}{2}\left(\frac{\varepsilon - \varepsilon_{\mathrm{D}}}{2\lambda\hbar^3 \cos 3\theta}\right)^2 - \sqrt{\frac{1}{27}\left(\frac{\hbar v_{\mathrm{F}}}{2\lambda\hbar^3 \cos 3\theta}\right)^6 + \frac{1}{4}\left(\frac{\varepsilon - \varepsilon_{\mathrm{D}}}{2\lambda\hbar^3 \cos 3\theta}\right)^4}\right|}. \end{aligned} \tag{1.37}$$

Furthermore,

$$\frac{\mathrm{d}f}{\mathrm{d}k} = \mp \frac{(\hbar v_{\mathrm{F}})^2 k + 12\lambda^2 \hbar^6 k^5 \cos^2 3\theta}{\sqrt{(\hbar v_{\mathrm{F}})^2 k^2 + 4\lambda^2 \hbar^6 k^6 \cos^2 3\theta}}, \tag{1.38}$$

so

$$d(\varepsilon) = \frac{1}{(2\pi)^2} \int_0^{2\pi} \mathrm{d}\theta \left[k \frac{\sqrt{(\hbar v_{\mathrm{F}})^2 + 4\lambda^2 \hbar^6 k^4 \cos^2 3\theta}}{(\hbar v_{\mathrm{F}})^2 + 12\lambda^2 \hbar^6 k^4 \cos^2 3\theta}\right]_{k=k_i}. \tag{1.39}$$

Recognizing that since $\delta\big(\varepsilon - \varepsilon(k)\big)$, effectively $E_{\pm}(\mathbf{k}) = \varepsilon$, so

$$\sqrt{(\hbar v_{\mathrm{F}})^2 k^2 + (2\lambda\hbar^3 \cos 3\theta)^2 k^6} = \pm\big(E_{\pm}(\mathbf{k}) - \varepsilon_{\mathrm{D}}\big) = \pm(\varepsilon - \varepsilon_{\mathrm{D}}), \tag{1.40}$$

or

$$(\hbar v_{\mathrm{F}})^2 k^2 + (2\lambda\hbar^3 \cos 3\theta)^2 k^6 = (\varepsilon - \varepsilon_{\mathrm{D}})^2, \tag{1.41}$$

and

$$\begin{aligned}(\hbar v_{\mathrm{F}})^2 k^2 + 12(\lambda\hbar^3 \cos 3\theta)^2 k^6 &= (\hbar v_{\mathrm{F}})^2 k^2 + (2\lambda\hbar^3 \cos 3\theta)^2 k^6 + 8(\lambda\hbar^3 \cos 3\theta)^2 k^6 \\ &= (\varepsilon - \varepsilon_{\mathrm{D}})^2 + 8(\hbar^3\lambda \cos 3\theta)^2 k^6\end{aligned} \tag{1.42}$$

the density of states reduces to (choosing the physical positive solution above)

$$d(\varepsilon) = \frac{\varepsilon - \varepsilon_{\mathrm{D}}}{(2\pi)^2} \int_0^{2\pi} \mathrm{d}\theta \left[\frac{k^2}{(\varepsilon - \varepsilon_{\mathrm{D}})^2 + 8\lambda^2\hbar^6 k^6 \cos^2 3\theta}\right]_{k=k_i}. \tag{1.43}$$

Solving for k_i in Eq. (1.34) and inserting these solutions into the above equation is analytically intractable, so instead we resort to a numerical calculation of d. The result is shown as the blue curve in Fig. 1.11. This plot can be compared to the no-field tunneling conductance line in [8, Fig. 3] shown in Fig. 1.12, and the profiles is seen to match fairly well. Notice that the in Fig. 1.12 is located at about -230 meV, whereas the Dirac-point energy used in our numerical calculations in -330 meV. We also notice that the no-warping DOS is changed radically when warping is included as seen in Fig. 1.11, where the no-warping DOS starts deviating from the warping DOS at about $E = -200$ meV. At the Fermi surface, the warping DOS is only about 2/3 of the no-warping DOS.

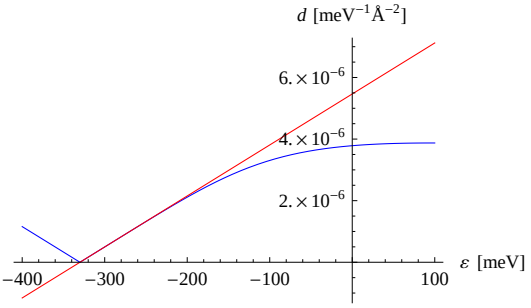

Figure 1.11: The DOS without warping (red curve) from Eq. (1.31) and the DOS with warping (blue curve) found numerically from Eq. (1.43).

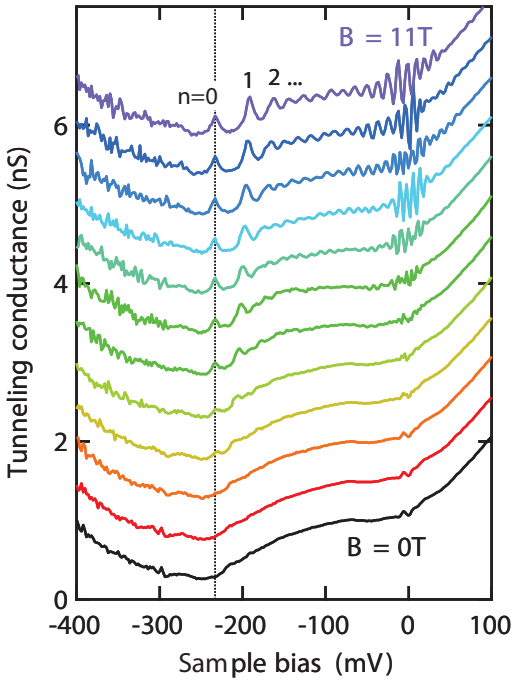

Figure 1.12: STM data done on Bi_2Se_3 from [8] for magnetic fields from $B = 0$ T to $B = 11$ T.

2 Landau levels

In this chapter the problem that will be addressed is how an external magnetic field will change the properties of a topological insulator. In particular, how the eigenenergies and eigenstates are affected, but also how to deal with both the warping effect *and* the effects induced by a magnetic field. The results in form of a DOS are then compared to data from the literature.

Before diving into the investigation of Landau levels in systems with strong spin–orbit coupling let us recapitulate what we know about Landau levels in a well-known two-dimensional electron gas constituting a *conventional* metal in the presence of a strong magnetic field.

2.1 Landau levels in a conventional two-dimensional electron gas

When a strong magnetic field is applied perpendicular to the surface of a two-dimensional conducting material, the orbital motion of the electrons becomes completely quantized and the energy spectrum becomes discrete. These electronic levels are called Landau levels and it is the purpose of this section to find the energies of these levels. Notice that in quantizing the energy spectrum, we actually quantize Bloch waves. So the periodic lattice potential is of course still present, but it does not enter in the calculations of the Landau levels.

The starting point is the free-particle Hamiltonian,

$$H = \frac{1}{2m}\mathbf{p}^2. \tag{2.1}$$

The effect of the magnetic field is taken into account through the magnetic vector potential $\mathbf{A}$ which modifies the momentum $\mathbf{p}$,

$$\mathbf{p} \to \boldsymbol{\pi} = -\mathrm{i}\hbar\boldsymbol{\nabla} + e\mathbf{A}. \tag{2.2}$$

Choosing the Landau gauge, $\mathbf{A} = Bx\hat{\mathbf{y}}$, the Schrödinger equation now reads

$$H\psi = \frac{1}{2m}\big(p_x^2 + (p_y + eBx)^2\big)\psi = \frac{1}{2m}\big(p_x^2 + p_y^2 + 2eBxp_y + (eBx)^2\big)\psi = E\psi. \tag{2.3}$$

The solutions to

$$\frac{1}{2m}p_y^2\psi_y(y) = E_y\psi_y(y), \tag{2.4}$$

are plane wave solutions, $\psi_y(y) = \mathrm{e}^{\mathrm{i}k_y y}$. Guessing a product solution,

$$\psi(\mathbf{r}) = \psi_x(x)\psi_y(y), \tag{2.5}$$

and inserting this solution into Eq. (2.3) yields

$$\left[-\frac{\hbar^2}{2m}\frac{\partial^2}{\partial x^2} + (eB)^2\left(x + \frac{\hbar k_y}{eB}\right)^2\right]\psi_x = E\psi_x. \tag{2.6}$$

This is the equation for an electron with energy E confined in a harmonic oscillator potential

$$V(x) = \frac{1}{2}m\omega_{\mathrm{c}}^2(x + x_0)^2 \tag{2.7}$$

with its minimum shifted to

$$x_0 = -\frac{\hbar k_y}{eB} = -l_B^2 k_y, \tag{2.8}$$

where the magnetic length,

$$l_B \equiv \sqrt{\frac{\hbar}{eB}}, \tag{2.9}$$

was introduced. The energy spectrum for a simple harmonic quantum oscillator is known to be

$$E_n = \hbar\omega_{\mathrm{c}}\left(n + \frac{1}{2}\right), \qquad n = 0, 1, 2, \ldots \tag{2.10}$$

where n is the Landau-level index, and

$$\omega_{\mathrm{c}} \equiv \frac{eB}{m} \tag{2.11}$$

is the cyclotron frequency. Furthermore, the separation energy of the Landau levels,

$$E_{n+1} - E_n = \hbar\omega_{\mathrm{c}}, \tag{2.12}$$

is seen to be independent of the Landau-level index n, i.e. the energy spectrum is equidistant. We know the wave function of a simple harmonic quantum oscillator to be

$$\psi_x(x) = \left(\frac{eB}{\pi\hbar}\right)^{1/4} \frac{1}{2^{n/2}\sqrt{n!}} \exp\left[-\frac{(x+x_0)^2}{2l_B^2}\right] H_n\big((x+x_0)/l_B\big), \tag{2.13}$$

where H_n is the nth order Hermite polynomial, so the wave function for the nth LL is

$$\psi_n(x,y) \equiv \psi_{x,n}(x)\psi_{y,n}(y) = \left(\frac{eB}{\pi\hbar}\right)^{1/4} \frac{1}{2^{n/2}\sqrt{n!}}\, \mathrm{e}^{\mathrm{i}k_y y} \exp\left[-\frac{(x-x_0)^2}{2l_B^2}\right] H_n\big((x-x_0)/l_B\big). \tag{2.14}$$

The magnetic length l_B can be interpreted as the radius of the classical zero-point-energy cyclotron orbit. This is seen by equating the zero-mode energy,

$$E_0 = \frac{\hbar\omega_{\mathrm{c}}}{2} = \frac{\hbar eB}{2m}, \tag{2.15}$$

with the free-particle energy,

$$E_k = \frac{\hbar^2 k^2}{2m}, \tag{2.16}$$

and solving for $l_B = k^{-1}$.

To summarize, electrons with a quadratic dispersion relation,

$$E(k) = E_0 + \frac{\hbar^2}{2m}k^2, \tag{2.17}$$

which are confined in two dimensions and placed in a strong magnetic field, have their motion quantized into cyclotron orbits. In this case, with an strong applied magnetic field B, the energy spectrum—continuous in k—of the electrons is quantized into a discrete, equidistant energy spectrum,

$$E_n = \left(\frac{1}{2} + n\right)\hbar\omega_{\mathrm{c}}. \tag{2.18}$$

2.2 Landau levels for surface-state Dirac electrons

We now turn to the case of applying an external magnetic field to a topological insulator in the low-energy regime, where the electrons obey the Dirac equation.

2.2.1 Energy spectrum

First, in the absence of an external magnetic field, we will assume that we can neglect the warping term, which breaks the in-plane rotation symmetry, i.e. $\lambda = 0$. The starting point is then the surface Hamiltonian of the low-energy surface states on a topological insulator as given by [3],

$$H = \varepsilon_{\mathrm{D}}\tau_0 + H_{\mathrm{free}} + H_{\mathrm{R}}, \tag{2.19}$$

where

$$H_{\mathrm{free}} = \frac{\hbar^2}{2m^*}k^2\tau_0 \tag{2.20}$$

is the free electron Hamiltonian with the chemical potential $\mu = -\varepsilon_{\mathrm{D}}$ with ε_{D} being the energy at the Dirac point,

$$H_{\mathrm{R}} = \hbar v_{\mathrm{F}}(\tau_x k_y - \tau_y k_x) \tag{2.21}$$

is the Rashba Hamiltonian. Notice that free-electron Hamiltonian has been included in order to obtain a more general result. The motivation for including this term is that the bulk-state electrons can have a Rashba-split quadratic dispersion relation as we will see later on, so in order to describe this band structure a k^2 term has to be included. On matrix form the surface Hamiltonian for electrons residing in the xy plane is then

$$H = \varepsilon_{\mathrm{D}}\tau_0 + H_{\mathrm{free}} + H_{\mathrm{R}} = \begin{pmatrix} \varepsilon_{\mathrm{D}} + \frac{\hbar^2}{2m^*}k^2 & \hbar v_{\mathrm{F}}(k_y + \mathrm{i}k_x) \\ \hbar v_{\mathrm{F}}(k_y - \mathrm{i}k_x) & \varepsilon_{\mathrm{D}} + \frac{\hbar^2}{2m^*}k^2 \end{pmatrix}. \tag{2.22}$$

When applying an external magnetic field, there are two effects which contributes to the Landau quantization of the energy levels, namely the orbital effect coupling the orbital angular momentum and the magnetic field,

$$H_{\mathrm{orbital}} = \frac{\mu_{\mathrm{B}}}{\hbar}\mathbf{L}\cdot\mathbf{B}, \tag{2.23}$$

and the Zeeman effect from an external magnetic field, coupling the spin angular momentum and the magnetic field,

$$H_{\mathrm{Zeeman}} = \frac{\mu_{\mathrm{B}}}{2}g\boldsymbol{\tau}\cdot\mathbf{B}. \tag{2.24}$$

The orbital effect of the magnetic field will as in the previous section give the momentum a magnetic contribution, such that the momentum is changed into the canonical momentum,

$$\mathbf{k} \to \boldsymbol{\kappa} = \mathbf{k} + \frac{e}{\hbar}\mathbf{A}, \tag{2.25}$$

Since the raising and lowering operator for the momentum is

$$\kappa_{\pm} \equiv \kappa_x \pm \mathrm{i}\kappa_y, \tag{2.26}$$

and these can be represented by the creation operator $a^\dagger$ and the annihilation operator a,

$$\kappa_+ \to \pi_+ = \frac{\sqrt{2}}{l_B}a^\dagger, \tag{2.27}$$

$$\kappa_- \to \pi_- = \frac{\sqrt{2}}{l_B}a, \tag{2.28}$$

where $l_B = \sqrt{\hbar/eB}$ is the magnetic length, using Peierls substitution one gets

$$\kappa_y + \mathrm{i}\kappa_x = \mathrm{i}\kappa_- \quad \to \quad \mathrm{i}\frac{\sqrt{2}}{l_B}a, \tag{2.29}$$

$$\kappa_y - \mathrm{i}\kappa_x = -\mathrm{i}\kappa_+ \quad \to \quad -\mathrm{i}\frac{\sqrt{2}}{l_B}a^\dagger, \tag{2.30}$$

upon chosing the Landau gauge $\mathbf{A} = (0, B_z x, 0)$, which preserves the translational invariance along the y direction. We also have the squared in-plane momentum,

$$\kappa^2 = \kappa_x^2 + \kappa_y^2 = \frac{1}{2}(\kappa_+\kappa_- + \kappa_-\kappa_+) = \frac{1}{l_B^2}(a^\dagger a + aa^\dagger) = \frac{2}{l_B^2}\left(a^\dagger a + \frac{1}{2}\right), \tag{2.31}$$

where the canonical commutation relation, $[a, a^\dagger] = 1$, was used in the last equality. These results inserted into Eq. (2.22) yield

$$H_{\text{orbital}} = \begin{pmatrix} \varepsilon_{\text{D}} + \frac{\hbar^2}{2m^*}\frac{2}{l_B^2}\left(a^\dagger a + \frac{1}{2}\right) & \mathrm{i}\frac{\sqrt{2}}{l_B}\hbar v_{\text{F}} a \\ -\mathrm{i}\frac{\sqrt{2}}{l_B}\hbar v_{\text{F}} a^\dagger & \varepsilon_{\text{D}} + \frac{\hbar^2}{2m^*}\frac{2}{l_B^2}\left(a^\dagger a + \frac{1}{2}\right) \end{pmatrix}. \tag{2.32}$$

As proposed in [3] we use an ansatz wave function, which is a product solution consisting of a plane wave solution in the y-direction, because of the translational invariance in this direction, and a quantum harmonic oscillator solution in the x-direction,

$$\Psi(x, y) = \frac{1}{\sqrt{|\phi_{N-1}(x)|^2 + |\phi_N(x)|^2}} \begin{pmatrix} \mathrm{e}^{\mathrm{i}k_y y}\,\phi_{N-1}(x) \\ \mathrm{e}^{\mathrm{i}k_y y}\,\phi_N(x) \end{pmatrix} \tag{2.33}$$

where ϕ_n is a nth quantum harmonic oscillator eigenfunction in the x-direction,

$$\phi_n(x) = \left(\frac{eB}{\pi\hbar}\right)^{1/4} \frac{1}{2^{n/2}\sqrt{n!}} \exp\left[-\frac{(x - k_y l_B^2)^2}{2l_B^2}\right] H_n\big((x - k_y l_B^2)/l_B\big). \tag{2.34}$$

where n is the Landau-level index. Operating on these functions with raising or lowering operators changes the level n according to

$$a^\dagger\,\phi_n = \sqrt{n+1}\,\phi_{n+1}, \tag{2.35}$$

$$a\,\phi_n = \sqrt{n}\,\phi_{n-1}, \tag{2.36}$$

and in particular, for the later calculations, we have the occupation number operations,

$$a^\dagger a\,\phi_n = n\,\phi_n, \tag{2.37}$$

$$a^\dagger a\,\phi_{n-1} = (n-1)\,\phi_{n-1}. \tag{2.38}$$

Using bra(c)ket notation one obtains

$$a = \sqrt{n}|n-1\rangle\langle n|, \tag{2.39}$$

$$a^\dagger = \sqrt{n}|n\rangle\langle n-1|, \tag{2.40}$$

$$a^\dagger a = n|n\rangle\langle n|. \tag{2.41}$$

The Hamiltonian for the orbital effect can be written in the basis of the quantum harmonic eigenstates, $|n-1\rangle$ and $|n\rangle$,

$$\begin{aligned} H_{\text{orbital}} &= \begin{pmatrix} \varepsilon_{\text{D}} + \frac{\hbar eB}{m^*}\left(a^\dagger a + \frac{1}{2}\right) & \mathrm{i}\sqrt{2\hbar eB}\,v_{\text{F}} a \\ -\mathrm{i}\sqrt{2\hbar eB}\,v_{\text{F}} a^\dagger & \varepsilon_{\text{D}} + \frac{\hbar eB}{m^*}\left(a^\dagger a + \frac{1}{2}\right) \end{pmatrix} \\ &= \left(\varepsilon_{\text{D}} + \frac{\hbar eB}{m^*}[a^\dagger a + 1/2]\right)|n-1\rangle\langle n-1| \\ &\quad + \left(\varepsilon_{\text{D}} + \frac{\hbar eB}{m^*}[a^\dagger a + 1/2]\right)|n\rangle\langle n| \\ &\quad + \mathrm{i}\sqrt{2\hbar eB}\,v_{\text{F}}\big(a|n\rangle\langle n| - a^\dagger|n-1\rangle\langle n-1|\big) \\ &= \begin{pmatrix} \varepsilon_{\text{D}} + \frac{\hbar eB}{m^*}\left((n-1) + \frac{1}{2}\right) & \mathrm{i}\sqrt{2\hbar eB}\,v_{\text{F}}\sqrt{n} \\ -\mathrm{i}\sqrt{2\hbar eB}\,v_{\text{F}}\sqrt{n} & \varepsilon_{\text{D}} + \frac{\hbar eB}{m^*}\left(n + \frac{1}{2}\right) \end{pmatrix}. \end{aligned} \tag{2.42}$$

In the case where the magnetic field points along the z axis, the Zeeman Hamiltonian is

$$H_{\text{Z}} = \frac{\mu_{\text{B}}}{2} g B \tau_z, \tag{2.43}$$

where $\mu_{\text{B}} = {}^{e\hbar}/_{2m_{\text{e}}}$ is the Bohr magneton for an electron with mass m_e. Including this Hamiltonian, the total Hamiltonian for the Landau-level surface states becomes

$$H = H_{\text{orbital}} + H_{\text{Z}} = \begin{pmatrix} \varepsilon_{\text{D}} + \frac{\hbar eB}{m^*}\left(n - \frac{1}{2}\right) + \frac{\mu_{\text{B}}}{2} gB & \mathrm{i}\sqrt{2\hbar eB}\,v_{\text{F}}\sqrt{n} \\ -\mathrm{i}\sqrt{2\hbar eB}\,v_{\text{F}}\sqrt{n} & \varepsilon_{\text{D}} + \frac{\hbar eB}{m^*}\left(n + \frac{1}{2}\right) - \frac{\mu_{\text{B}}}{2} gB \end{pmatrix}. \tag{2.44}$$

Diagonalization of the above Hamiltonian yields the energy spectrum,

$$E_{n,\pm} = \varepsilon_{\rm D} + \frac{\hbar eB}{m^*}n \pm \sqrt{\left(\frac{\mu_{\rm B}}{2}gB - \frac{\hbar eB}{2m^*}\right)^2 + 2e\hbar v_{\rm F}^2 nB}. \tag{2.45}$$

The Landau-quantized energy spectrum for surface-state Dirac electrons with helicity $\eta = \pm$ is then

$$E_{n,\eta} = \varepsilon_{\rm D} + \eta\sqrt{\left(\frac{\mu_{\rm B}}{2}g_{\rm s}B\right)^2 + 2e\hbar v_{\rm F}^2 nB}, \qquad n = 0, 1, 2, \ldots. \tag{2.46}$$

$\eta = +$ is for electrons with positive helicity and $\eta = -$ is for electrons with negative helicity.

2.2.2 Properties of the quantized surface states

From the energy spectrum in Eq. (2.46), we see that the Zeeman energy acts as the mass term in the original Dirac equation, since its role is to split the energy bands into two branches. In the absence of a Zeeman splitting, the energy spectrum is therefore massless with electron–hole symmetry, and in this case the there exists a zero-mode exactly at the Dirac-point energy, i.e. $E_0 = \varepsilon_{\rm D}$. This zero-mode state is therefore independent of the field strength, which is different from the zero-mode in a conventional metal, where the groundstate energy is $E_{0,\text{conv.}} = \hbar\omega_{\rm c}/2$.

For bismuth selenide we obtain the off-diagonal contribution,

$$\varepsilon_{\text{off-diag.}} \equiv v_{\rm F}\sqrt{2\hbar eB} = 17.1\ \text{meV}\sqrt{B[T]}\sqrt{n}, \tag{2.47}$$

where

$$\varepsilon_{\rm SO} = \sqrt{2}\hbar v_{\rm F} l_B^{-1} \tag{2.48}$$

is an energy characteristic for the spin–orbit coupling. The Zeeman energy with $g = 8.4375$ is

$$\varepsilon_{\rm Z} = \frac{\mu_{\rm B}}{2}gB = 0.24\ \text{meV}B[T]. \tag{2.49}$$

The energy spectrum of the quantized surface-state levels Eq. (2.46) is plotted in Fig. 2.1.

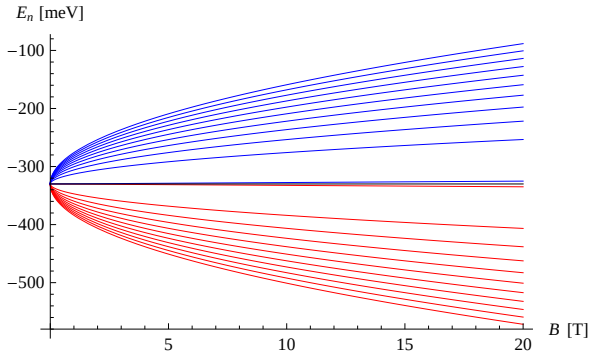

Figure 2.1: Landau levels for $n = 0, 1, 2, \ldots, 10$. Blue (red) lines represent energies for positive (negative) helicity. The Dirac point here lies at $\varepsilon_{\rm D} = -330$ meV indicated by a black line.

As a last remark on the properties of the quantized surface-state energy spectrum, we note that the energy difference between adjacent levels, $|n+1\rangle$ and $|n\rangle$, in the energy spectrum of Eq. (2.46) is

$$\begin{aligned} E_{n+1}^{\pm}(B) - E_n^{\pm}(B) &= \varepsilon_{\rm D} \pm \sqrt{\varepsilon_{\rm Z}^2 + \varepsilon_{\rm SO}^2(n+1)} - \left[\varepsilon_{\rm D} \pm \sqrt{\varepsilon_{\rm Z}^2 + \varepsilon_{\rm SO}^2 n}\right] \\ &= \pm\left[\sqrt{\varepsilon_{\rm Z}^2 + \varepsilon_{\rm SO}^2(n+1)} - \sqrt{\varepsilon_{\rm Z}^2 + \varepsilon_{\rm SO}^2 n}\right] \\ &= \pm\varepsilon_{\rm SO}\left[\sqrt{\left(\frac{\varepsilon_{\rm Z}}{\varepsilon_{\rm SO}}\right)^2 + 1 + n} - \sqrt{\left(\frac{\varepsilon_{\rm Z}}{\varepsilon_{\rm SO}}\right)^2 + n}\right]. \end{aligned} \tag{2.50}$$

Hence we see that the energy spectrum for Dirac electrons, the Landau levels are no longer equidistant as is the case for a conventional metal, where the energy difference is

$$\Delta E_{\text{conv.}} = \hbar\omega_{\rm c}, \tag{2.51}$$

where $\omega_{\rm c}$ is the cyclotron frequency.

2.3 Landau levels with warping

The analytical expression for the surface-state Hamiltonian with the warping is

$$H_{\text{sur}} = \begin{pmatrix} \varepsilon_{\text{D}} + \varepsilon_{\text{Z}} + \lambda\hbar^3(\kappa_+^3 + \kappa_-^3) & \mathrm{i}\hbar v_{\text{F}}\kappa_- \\ -\mathrm{i}\hbar v_{\text{F}}\kappa_+ & \varepsilon_{\text{D}} - \varepsilon_{\text{Z}} - \lambda\hbar^3(\kappa_+^3 + \kappa_-^3) \end{pmatrix}, \tag{2.52}$$

and then using the ladder operators

$$\kappa_+ \to \pi_+ = \frac{\sqrt{2}}{l_B} a^\dagger, \tag{2.53}$$

$$\kappa_- \to \pi_- = \frac{\sqrt{2}}{l_B} a, \tag{2.54}$$

we obtain the Hamiltonian for the surface states expressed by the ladder operators,

$$H_{\text{sur}} = \begin{pmatrix} \varepsilon_{\text{D}} + \varepsilon_{\text{Z}} + \lambda\hbar^3 \left(\frac{\sqrt{2}}{l_B}\right)^3 \left((a^\dagger)^3 + a^3\right) & \mathrm{i}\frac{\sqrt{2}}{l_B}\hbar v_{\text{F}} a \\ -\mathrm{i}\frac{\sqrt{2}}{l_B}\hbar v_{\text{F}} a^\dagger & \varepsilon_{\text{D}} - \varepsilon_{\text{Z}} - \lambda\hbar^3 \left(\frac{\sqrt{2}}{l_B}\right)^3 \left((a^\dagger)^3 + a^3\right) \end{pmatrix}. \tag{2.55}$$

Realizing the fact that the terms containing cubed ladder operators, a^3 and $(a^\dagger)^3$, describe an anharmonic oscillator, which is not analytically solvable, leaves us no hope of finding an analytical expression for the eigenenergies of the Hamiltonian above either. Rather we shall resort to a numerical treatment of the problem. To include the warping effect we choose a numerical model representing a $n \times n$ dimensional Hilbert space. This means that instead of applying ladder operators on a quantum oscillator state $|n\rangle$ as in Eqs. (2.35) and (2.36), we simply let the ladder operators represent the states themselves, now as $n \times n$ matrices. The *Mathematica* codes which were used to generate these eigenenergies are given in Sec. A.5.

The energy spectrum for the first 200 Landau levels is shown in Fig. 2.2, with and without warping. When the warping is turned off the numerically found energy spectrum (green lines) coincides with the analytically found energy spectrum in Eq. (2.46), shown as black curves. At high energies—i.e. high n—the warped positive (negative) levels have higher (lower) energy in comparison with the corresponding unwarped levels.

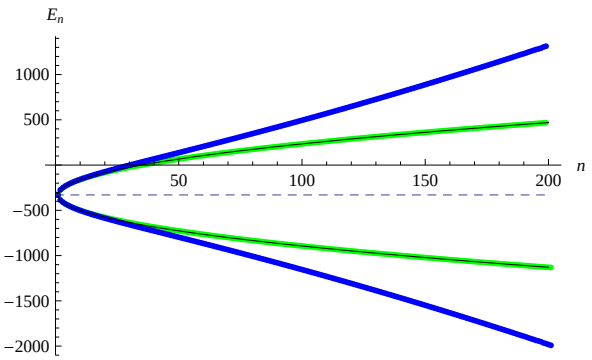

Figure 2.2: Landau levels in the numerical treatment of the warping problem. Levels with warping, shown as blue lines which curve away from the n-axis, and levels without warping, shown as green lines which curve towards the n-axis. The black curves indicate the analytically found energy for the quantized Landau levels. The dashed line marks the Dirac-point energy.

2.4 Density of states in magnetic field: Quantum oscillations

In Sec. 1.4 the DOS of topological-insulator in absence of an external field was investigated. In this section we progress by taking a magnetic field into consideration and see how the DOS is changed.

2.4.1 DOS for Dirac electrons in magnetic field

In the article of [8] the tunneling conductance of Bi_2Se_3 as a function of the sample bias is shown to oscillate wildly around the Fermi-surface energy for nonzero magnetic fields, the strongest being $B = 11$ T. The authors suggests that this effect comes from the the overlap of the bulk *conduction band-induced* surface states (a.k.a. 2DEG states) and the *topological* surface states. At the surface of the material the bulk bands bend, and this results in bound states at the surface of the material. This is illustrated in Fig. 2.3.

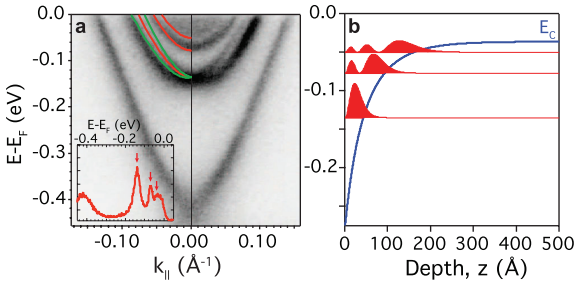

Figure 2.3: (**a**) Measurements of multiple 2DEG states and the topological surface states in Bi_2Se_3. Model Poisson–Schrödinger calculations reproduce of the 2DEG states (red line) in the surface quantum well. These 2DEG states are Rashba-split by $\alpha = 0.36$ meV Å. (**b**) Bending of the bulk bands (blue line) near the surface of the material with modulus-squared wave functions of the confined states. From [9].

This paves the way for the 2DEG bands to mix with the topological surface bands near the surface of the material. Treating the 2DEG states in the same way as the topological surface states, we get for the pre-magnetized dispersion relation,

$$E^{\mathrm{b}}_{\pm,B=0}(k) = \gamma_0 \pm \alpha k + \gamma k^2, \tag{2.56}$$

the bulk-state Hamiltonian in an applied magnetic field B becomes quantized through the Landau-level index n,

$$H_{\mathrm{b}} = \begin{pmatrix} \gamma_0 + \frac{2eB}{\hbar}\gamma\left(n - \frac{1}{2}\right) + \frac{\mu_{\mathrm{B}}}{2} g_{\mathrm{b}} B & \mathrm{i}\sqrt{\frac{2eB}{\hbar}}\alpha\sqrt{n} \\ -\mathrm{i}\sqrt{\frac{2eB}{\hbar}}\alpha\sqrt{n} & \gamma_0 + \frac{2eB}{\hbar}\gamma\left(n + \frac{1}{2}\right) - \frac{\mu_{\mathrm{B}}}{2} g_{\mathrm{b}} B \end{pmatrix}. \tag{2.57}$$

Notice that, as mentioned earlier in connection with the derivation of the Landua-quantized energy spectrum, that we have now included the k^2 contribution, and hence the eigenenergies of bulk conduction band-induced Hamiltonian are similar to those given by Eq. (2.45), and upon making the relevant substitutions we obtain

$$E^{\mathrm{b}}_{n,\pm}(B) = \gamma_0 + \frac{2eB}{\hbar}\gamma n \pm \sqrt{\left(\frac{\mu_{\mathrm{B}}}{2} g_{\mathrm{b}} B - \frac{eB}{\hbar}\gamma\right)^2 + \frac{2eB}{\hbar}\alpha^2 n}. \tag{2.58}$$

The energy spectrum for the topological surface-state electrons in the low-energy regime is

$$E^{\mathrm{s}}_{n,\pm}(B) = \varepsilon_{\mathrm{D}} \pm \sqrt{\left(\frac{\mu_{\mathrm{B}}}{2} g_{\mathrm{s}} B\right)^2 + 2eB\hbar v_{\mathrm{F}}^2 n}. \tag{2.59}$$

The density of states per unit area for the topological surface electrons in an external magnetic field B—assuming no thermal and collisional smearing—is simply represented by peaks at each Landau-level index n,

$$d(\varepsilon) = \frac{2eB}{2\pi\hbar}\sum_n^{\infty} \delta(\varepsilon - E_{n,\pm}). \tag{2.60}$$

But in real life, scattering processes will broaden the delta peaks so the Landau levels are described by a collision-broadened Lorentzian profile instead, i.e.

$$\delta(\varepsilon - E_{n,\pm}) \;\rightarrow\; \frac{1}{\pi}\frac{\hbar\Gamma}{(\varepsilon - E_{n,\pm}(\mathbf{k}))^2 + (\hbar\Gamma)^2}, \tag{2.61}$$

with Γ being the scattering rate, i.e. the width of the broadening profile.

The total DOS is the sum of the density of surface states and the density of bulk conduction-band states,

$$d_{\mathrm{tot}}(\varepsilon) = d_{\mathrm{s}}(\varepsilon) + d_{\mathrm{b}}(\varepsilon) = \frac{2eB}{2\pi\hbar}\sum_{n}^{N}\frac{1}{\pi}\frac{\hbar\Gamma}{(\varepsilon - E^{\mathrm{s}}_{n,\pm})^2 + (\hbar\Gamma)^2} + \frac{2eB}{2\pi\hbar}\sum_{n}^{N}\frac{1}{\pi}\frac{\hbar\Gamma}{(\varepsilon - E^{\mathrm{b}}_{n,\pm})^2 + (\hbar\Gamma)^2}. \tag{2.62}$$

Here we have cut the sum off at some integer N toa allow for computational implementation. Using the following values,

$$\gamma_0 = -90 \text{ meV}, \tag{2.63}$$

$$\alpha = 360 \text{ meV Å}, \tag{2.64}$$

$$\gamma = 19\,053 \text{ meV Å}^2, \tag{2.65}$$

from P. Hofmann (priv. comm.) and choosing $\Gamma = 5 \text{ meV}/\hbar$, the numerical calculation with $N = 2002$ of the DOS in Eq. (2.62) is shown in Fig. 2.4. The Landau levels for the topological surface-state electrons are clearly seen around the Dirac point at $\varepsilon_{\mathrm{D}} = -330$ meV all the way up to γ_0. From here on the density of the bulk conduction-band states starts to contribute to the total DOS, and this gives rise to a number of pronounced peaks. It is unclear whether this effect is a quantum-oscillation effect, but one could speculate that the 2DEG states and the surface states couple through impurity-induced interband scattering. This effect is maybe what is displayed in the Fermi-level DOS of Fig. 2.4.

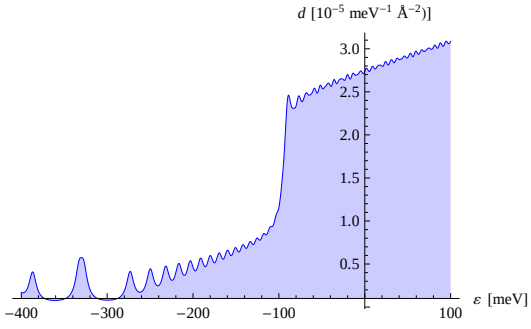

Figure 2.4: The total DOS for Landau levels of the both surface states and bulk states as in Eq. (2.62) without the warping effect. The eigenenergies used are analytically found.

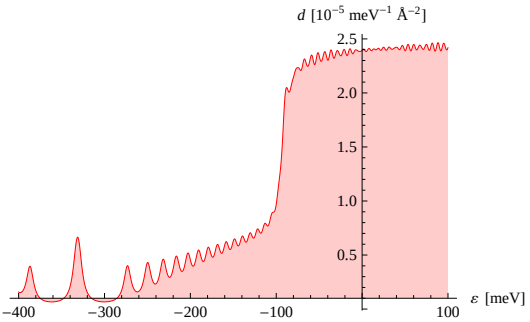

Figure 2.5: The total DOS for warped Landau levels of the both surface states and bulk states as in Eq. (2.62). The eigenenergies used are numerically found.

2.4.2 DOS for topological-insulator electrons with warping in magnetic field

Including the warping effect by using the warped energy spectrum obtained from the numerical model in Sec. 2.3, we get the result shown in Fig. 2.5. To obtain the bulk conduction band-state energies we have added $eB\gamma/\hbar$ in the diagonal of the Hamiltonian in Eq. (2.55) and substituted $\hbar v_{\mathrm{F}}$ with α and ε_{D} with γ_0. As in Fig. 2.4 the Landau levels of the surface-state electrons are clearly seen from ε_{D} up to γ_0. At γ_0 the DOS of the bulk-induced surface states starts to contribute to the total DOS, which results in a steep increase in the DOS at γ_0. After the bulk-induced states set in, the total DOS seems to linearly increase, with several peaks in the wake. Qualitatively, this is in good agreement with the result in Fig. 1.11, where the warping has a diminishing effect on the no-field DOS.

Unfortunately, comparison of the plots in Figs. 2.4 and 2.5, as seen in Fig. 2.6 and Fig. 2.7, does not reveal that the DOS at the Fermi surface has changed in any *particular* way due to warping effects. However, we do notice that the warping pushes the surface Landau levels towards higher energies, starting at about $E = -200$ meV.

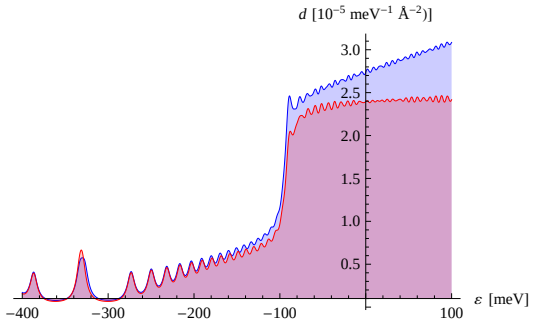

Figure 2.6: The total DOS without the warping effect (blue) from Fig. 2.4 and with the warping effect (red) from Fig. 2.5.

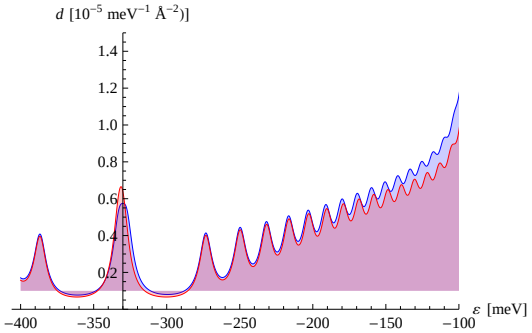

Figure 2.7: A zoom-in of the low-energy regime of Fig. 2.6. With warping: blue line; without warping: red line.

3 Semiclassical approach to spin–momentum locking effects

3.1 Berry's phase and the anomalous velocity

The concept of Berry's phase in quantum mechanics together with the classical equations of motion form a simple semiclassical theory of the dynamics of electrons in a solid. The advantage of semiclassical theories is its transparency and simplicity, which makes it ideal for explaining how physical results come about. By using the semiclassical approach one can get a good physical intuition without having to start the more technical machinery of purely quantum-mechanical methods, such as those based on the Kubo formula in linear response theory. In this section we will first review a number of results for the semiclassical theory, which will then be used afterwards on topologically insulating systems.

3.1.1 The concept of Berry's phase

We first consider a time-independent Hamiltonian H [10]. If a particle starts in the nth eigenstate, described by the wave function ψ_n, which obeys the Schrödinger equation,

$$H\psi_n = E_n\psi_n, \tag{3.1}$$

it will remain in that state, i.e. ψ_n designates a stationary state. The full wave function for such a state at time t is then

$$\Psi_n(t) = \psi_n \, \mathrm{e}^{-\mathrm{i}E_n t/\hbar}. \tag{3.2}$$

Now, if the Hamiltonian itself acquires a time dependence, the eigenfunction and eigenvalues will also be time-dependent, such that instead of Eq. (3.1) we are considering

$$H(t)\psi_n(t) = E_n(t)\psi_n(t). \tag{3.3}$$

It can be shown that the full wave function in the adiabatic approximation (which says that H varies so slowly in time, that $\dot{H} \approx 0$) then reads

$$\Psi_n(t) = \mathrm{e}^{\mathrm{i}\left(\theta_n(t)+\gamma_n(t)\right)} \, \psi_n(t). \tag{3.4}$$

Here the first phase,

$$\theta_n(t) \equiv -\frac{1}{\hbar}\int_0^t \mathrm{d}t' \, E_n(t'), \tag{3.5}$$

is called the dynamic phase, and it is merely a generalization of the usual time evolution factor $\mathrm{e}^{-\mathrm{i}E_n t/\hbar}$. The second phase in Eq. (3.4),

$$\gamma_n(t) = \int_0^t \mathrm{d}t' \, \langle\psi_n(t')|\mathrm{i}\partial_{t'}\psi_n(t')\rangle, \tag{3.6}$$

is called the geometric phase. Hence in the adiabatic approximation, the full wave function acquires an additional phase, the geometric phase, γ_n.

Now, upon taking the system described by $\psi_n(t)$ around in a closed trajectory whose period is denoted by T, the accumulated geometric phase becomes what is known as Berry's phase (in this thesis a 'B' will always indicate a quantity associated with Berry's phase),

$$\gamma_{\mathrm{B},n} \equiv \gamma_n(T) = \int_0^T \mathrm{d}t \, \langle\psi_n(t)|\mathrm{i}\partial_t\psi_n(t)\rangle. \tag{3.7}$$

Hence Berry's phase only depends on the path taken, not e.g. on how fast is is traced out, as long as the adiabatic approximation is not violated. A process in which a system does not return to its original state when locomoted around a closed loop, is said to be nonholonomic. Hence Berry's phase is nonzero for a nonholonomic process, e.g. the process of transporting of a spin around in a magnetic field.

The wave function $\psi_n(t)$ depends on the time t because there are some parameters,

$$\mathbf{R}(t) = (R_1(t), R_2(t), \ldots), \tag{3.8}$$

in the Hamiltonian which gives it a time dependence. Hence we consider the more general problem,

$$H(\mathbf{R}(t))\psi_n(\mathbf{R}(t)) = E_n(\mathbf{R}(t))\psi_n(\mathbf{R}(t)). \tag{3.9}$$

The time derivative in Eq. (3.7) can then be written as

$$\frac{\partial \psi_n}{\partial t} = \frac{\partial \psi}{\partial R_1}\dot{R}_1 + \frac{\partial \psi}{\partial R_2}\dot{R}_2 + \cdots + \frac{\partial \psi}{\partial R_N}\dot{R}_N = \partial_{\mathbf{R}}\psi_n \cdot \dot{\mathbf{R}}, \tag{3.10}$$

and the geometric phase can accordingly be recast as

$$\gamma_n(t) = \int_{\mathbf{R}(0)}^{\mathbf{R}(t)} \mathrm{d}\mathbf{R} \cdot \langle \psi_n(\mathbf{R}) | \mathrm{i}\partial_{\mathbf{R}} \psi_n(\mathbf{R}) \rangle. \tag{3.11}$$

If the Hamiltonian is periodic with the time T, Berry's phase is now

$$\gamma_{\mathrm{B},n} = \oint \mathrm{d}\mathbf{R} \cdot \langle \psi_n(\mathbf{R}) | \mathrm{i}\partial_{\mathbf{R}} \psi_n(\mathbf{R}) \rangle. \tag{3.12}$$

By Stokes' theorem, the above line integral can be written as an integral over a surface in R space,

$$\gamma_{\mathrm{B},n} = \int \mathrm{d}\mathbf{S}_R \cdot (\partial_{\mathbf{R}} \times \langle \psi_n(\mathbf{R}) | \mathrm{i}\partial_{\mathbf{R}} \psi_n(\mathbf{R}) \rangle). \tag{3.13}$$

In the case where the parameter space is identical to the crystal momentum space, so

$$\mathbf{R} \to \mathbf{k} = (k_x, k_y, k_z), \tag{3.14}$$

Berry's phase in Eqs. (3.12) and (3.13) is reminiscient to the magnetic flux in terms of the magnetic vector,

$$\Phi_{\mathrm{M}} = \oint \mathrm{d}\mathbf{r} \cdot \mathbf{A} = \int \mathrm{d}\mathbf{S} \cdot \mathbf{B}. \tag{3.15}$$

This means that one can think of Berry's phase as the 'flux' of a 'magnetic field', called Berry's curvature,

$$\mathbf{B}_{\mathrm{B},n}(\mathbf{k}) = \partial_{\mathbf{k}} \times \mathbf{A}_n(\mathbf{k}), \tag{3.16}$$

through the closed-loop trajectory in parameter space, with a 'magnetic vector potential', called Berry's connection, being

$$\mathbf{A}_{\mathrm{B},n}(\mathbf{k}) \equiv \langle \psi_n | \mathrm{i}\partial_{\mathbf{k}} \psi_n \rangle. \tag{3.17}$$

Hence when $\mathbf{R} \to \mathbf{k}$, Berry's curvature acts as a magnetic field in Bloch space, establishing a kind of k-r duality between Berry's curvature $\mathbf{B}_{\mathrm{B},n}$ and the magnetic field $\mathbf{B}$. However, Berry's curvature originates from a source, which is unlike an electromagnetic field which has zero divergence, i.e. the flux lines do not start and end at a specific point, and hence it has no magnetic monopoles. The monopoles of Berry's curvature in Bloch bands correspond to the points of crossing of energy bands [11].

It then follows from Eqs. (3.12) and (3.13) that Berry's phase for the nth eigenstate is a line integral of $\mathbf{A}_{\mathrm{B},n}$ or a surface integral of $\mathbf{B}_{\mathrm{B},n}$ in momentum space,

$$\gamma_{\mathrm{B},n} = \oint \mathrm{d}\mathbf{k} \cdot \mathbf{A}_{\mathrm{B},n}(\mathbf{k}) = \int \mathrm{d}\mathbf{S}_k \cdot \mathbf{B}_{\mathrm{B},n}(\mathbf{k}). \tag{3.18}$$

3.1.2 Manifestation of Berry's curvature in electron bands

We shall now investigate what implications a nonzero Berry phase will have on electron dynamics, i.e. how the classical equations of motion are modified in nonholonomic systems. We therefore consider a two-dimensional electron gas describing a conventional metal with a quadratic dispersion relation, following [12] whose results were first shown in [13]. In such a system the electron dynamics can be described by a wave packet made by a superposition of Bloch wave functions,

$$\psi_{\mathbf{k}}(\mathbf{r}) = u_{\mathbf{k}}(\mathbf{r})\,\mathrm{e}^{\mathrm{i}\mathbf{k}\cdot\mathbf{r}}, \tag{3.19}$$

having its k-space center in $\mathbf{k}_\mathrm{c}$ and its nth band energy being E_n,

$$W_{\mathbf{r}_\mathrm{c}\mathbf{k}_\mathrm{c}}(\mathbf{r}) = \frac{1}{\sqrt{N}}\sum_{\mathbf{k}} w_{\mathbf{k}\mathbf{k}_\mathrm{c}}\,\mathrm{e}^{-\mathrm{i}e\mathbf{A}(\mathbf{r}_\mathrm{c})\cdot\mathbf{r}/\hbar}\,\mathrm{e}^{-\mathrm{i}\mathbf{k}\cdot\mathbf{r}_\mathrm{c}}\,\psi_{\mathbf{k}}(\mathbf{r}). \tag{3.20}$$

Here N is the number of unit cells (u.c.) in the system and $\mathbf{k}$ is the crystal momentum, which is summed over the first Brillouin zone. In the presence of a magnetic field $\mathbf{B}$ with associated magnetic vector potential $\mathbf{A}$, the wave packet acquires an additional phase, namely the Aharonov–Bohm phase,

$$\phi_\mathrm{AB}(\mathbf{r}_\mathrm{c}) \equiv \frac{e}{\hbar}\mathbf{A}(\mathbf{r}_\mathrm{c}). \tag{3.21}$$

This phase is included in order to avoid wild oscillations in the wave packet. The envelope function has the form

$$w_{\mathbf{k}_\mathrm{c}}(\mathbf{k}) = |w|_{\mathbf{k}-\mathbf{k}_\mathrm{c}}\,\mathrm{e}^{\mathrm{i}(\mathbf{k}-\mathbf{k}_\mathrm{c})\cdot\mathbf{A}_\mathrm{B}(\mathbf{k}_\mathrm{c})}, \tag{3.22}$$

where as indicated the amplitude function $|w|$ only depends on the the difference between $\mathbf{k}$ and $\mathbf{k}_\mathrm{c}$. The phase of the envelope function, containing Berry' connection, which comes from the k dependence of the periodic function $u_{\mathbf{k}}$ in the Bloch wave function,

$$\mathbf{A}_\mathrm{B}(\mathbf{k}_\mathrm{c}) \equiv \int_\mathrm{u.c.} \mathrm{d}\mathbf{r}\, u^*_{\mathbf{k}_\mathrm{c}}(\mathbf{r})\mathrm{i}\partial_{\mathbf{k}} u_{\mathbf{k}_\mathrm{c}}(\mathbf{r}) \equiv \langle u_{\mathbf{k}_\mathrm{c}}|\mathrm{i}\partial_{\mathbf{k}_\mathrm{c}} u_{\mathbf{k}_\mathrm{c}}\rangle, \tag{3.23}$$

carries information about the actual spatial location of the wave packet, and it is chosen in such a way as to ensure that the wave packet is indeed always centered around $\mathbf{r}_\mathrm{c}$,

$$\langle W_{\mathbf{r}_\mathrm{c}\mathbf{k}_\mathrm{c}}|\mathbf{r}(t)|W_{\mathbf{r}_\mathrm{c}\mathbf{k}_\mathrm{c}}\rangle = \mathbf{r}_\mathrm{c}(t). \tag{3.24}$$

Furthermore, we require that the envelope function is narrowly distributed around a center wave vector,

$$\mathbf{k}_\mathrm{c}(t) = \int_\mathrm{BZ} \mathrm{d}\mathbf{k}\,|w_{\mathbf{k}_\mathrm{c}(t)}(\mathbf{k})|^2\mathbf{k}, \tag{3.25}$$

such that one can speak of an approximate localization in k space. Hence we require that the wave numbers of the wave packet is much smaller than the width of the Brillouin zone. This means than the spatial extent of the wave packet will be much larger that an atomic spacing. On the other hand, the wave packet must not be too localized in k space, since we also want it to be approximately localized in real space around its center given in Eq. (3.24). The wave packet is also required to be normalized, i.e.

$$\langle W_{\mathbf{r}_\mathrm{c}\mathbf{k}_\mathrm{c}}|W_{\mathbf{r}_\mathrm{c}\mathbf{k}_\mathrm{c}}\rangle = 1, \tag{3.26}$$

which yields the requirement on the envelope function that

$$\int \mathrm{d}\mathbf{k}\,|w_{\mathbf{k}_\mathrm{c}}(\mathbf{k})|^2 = 1. \tag{3.27}$$

The equations of motion is given the the Euler–Lagrange equations,

$$\frac{\partial\mathcal{L}}{\partial\mathbf{r}_\mathrm{c}} = \frac{\mathrm{d}}{\mathrm{d}t}\frac{\partial\mathcal{L}}{\partial\dot{\mathbf{r}}_\mathrm{c}}, \tag{3.28}$$

$$\frac{\partial\mathcal{L}}{\partial\mathbf{k}_\mathrm{c}} = \frac{\mathrm{d}}{\mathrm{d}t}\frac{\partial\mathcal{L}}{\partial\dot{\mathbf{k}}_\mathrm{c}}, \tag{3.29}$$

with $\mathcal{L}$ being the effective Lagrangian for a system described by the Hamiltonian,

$$H = \frac{1}{2m}\left(\mathbf{p} + e\mathbf{A}(\mathbf{r})\right)^2 + U(\mathbf{r}), \tag{3.30}$$

where U is the periodic potential of the lattice, V is an external electric scalar potential and $\mathbf{A}$ is the magnetic vector potential. By the time-dependent variational principle, the effective Lagrangian of the wave packet in Eq. (3.20) moving in a weak electromagnetic field with real-space center $\mathbf{r}_\mathrm{c}$ and momentum-space center $\mathbf{k}_\mathrm{c}$,

$$\mathcal{L}(\mathbf{r}_\mathrm{c}, \dot{\mathbf{r}}_\mathrm{c}, \mathbf{k}_\mathrm{c}, \dot{\mathbf{k}}_\mathrm{c}, t) = \langle W_{\mathbf{r}_\mathrm{c}\mathbf{k}_\mathrm{c}} | \mathrm{i}\hbar \frac{\mathrm{d}}{\mathrm{d}t} | W_{\mathbf{r}_\mathrm{c}\mathbf{k}_\mathrm{c}} \rangle - \langle W_{\mathbf{r}_\mathrm{c}\mathbf{k}_\mathrm{c}} | \big(H - eV(\mathbf{r})\big) | W_{\mathbf{r}_\mathrm{c}\mathbf{k}_\mathrm{c}} \rangle, \tag{3.31}$$

is in [12] given as

$$\mathcal{L} = e\mathbf{r}_\mathrm{c} \cdot \dot{\mathbf{A}}(\mathbf{r}_\mathrm{c}) + \hbar \mathbf{k}_\mathrm{c} \cdot \dot{\mathbf{r}}_\mathrm{c} + \hbar \dot{\mathbf{k}}_\mathrm{c} \cdot \mathbf{A}_\mathrm{B}(\mathbf{k}_\mathrm{c}) + E_{\mathbf{k}_\mathrm{c}} + \frac{e}{2m} \mathbf{B} \cdot \mathbf{L}(\mathbf{k}_\mathrm{c}) - eV(\mathbf{r}_\mathrm{c}). \tag{3.32}$$

In what follows the $\mathbf{B} \cdot \mathbf{L}$ term will be neglected for simplicity, but for completeness a short discussion of it is found in Sec. A.2. By solving the Euler–Langrange equations above one finds the equation of motion for an electron in momentum space to be (we omit the 'c' on the real-space and momnetum-space positions for convenience)

$$\hbar \dot{\mathbf{k}} = -e\mathbf{E} - e\dot{\mathbf{r}} \times \mathbf{B}. \tag{3.33}$$

The wave-packet velocity of an electron with energy E in the given band, $\dot{\mathbf{r}}$, is a sum of the group velocity of the wave packet and an *anomalous velocity*,

$$\dot{\mathbf{r}} = \dot{\mathbf{r}}_\mathrm{g} + \dot{\mathbf{r}}_\mathrm{a} = \frac{1}{\hbar} \frac{\partial E}{\partial \mathbf{k}} - \dot{\mathbf{k}} \times \mathbf{B}_\mathrm{B}, \tag{3.34}$$

where the group velocity is

$$\dot{\mathbf{r}}_\mathrm{g} \equiv \frac{1}{\hbar} \frac{\partial E}{\partial \mathbf{k}}, \tag{3.35}$$

and the anomalous velocity is

$$\dot{\mathbf{r}}_\mathrm{a} \equiv -\dot{\mathbf{k}} \times \mathbf{B}_\mathrm{B} = -\begin{pmatrix} \dot{k}_y B_{\mathrm{B},z} - \dot{k}_z B_{\mathrm{B},y} \\ \dot{k}_z B_{\mathrm{B},x} - \dot{k}_x B_{\mathrm{B},z} \\ \dot{k}_x B_{\mathrm{B},y} - \dot{k}_y B_{\mathrm{B},x} \end{pmatrix}. \tag{3.36}$$

We recognize the $\mathbf{B}_\mathrm{B}$ in the anomalous velocity in Eq. (3.16) as Berry's curvature of the band in consideration.

From the expression in Eq. (3.23), Berry's connection can be interpreted as an intraband matrix element of the k-periodic part of the Bloch wave function $u_\mathbf{k}$ [14]. We also see that $\mathbf{A}_\mathrm{B}$ is nonzero only when $\mathbf{k}$ varies, which it does when a closed loop in momentum space is generated either by applying a magnetic field, which induces a cyclotron motion along a closed orbit in k space, or by applying an external electric field. From the semiclassical equations of motion this will make $\mathbf{k}$ evolve in time.

3.1.3 Conditions for the anomalous velocity to be nonzero

Since the anomalous velocity in Eq. (3.36) is proportional to the electric field and the magnetic field through $\dot{\mathbf{k}}$, the anomalous velocity can be neglected for small fields. This is why the group velocity in Eq. (3.35) is often a good approximation to linear order in the fields. But this is not always the case, so let us therefore see under exactly what conditions the anomalous velocity is nonzero.

Under the reversal of time, the velocity $\mathbf{v}$ and wave vector $\mathbf{k}$ change sign, while the electric field $\mathbf{E}$ is invariant, so

$$\mathbf{B}_\mathrm{B}(-\mathbf{k}) = -\mathbf{B}_\mathrm{B}(\mathbf{k}). \tag{3.37}$$

Under spatial inversion, $\mathbf{v}$, $\mathbf{k}$ and $\mathbf{E}$ change sign, so

$$\mathbf{B}_\mathrm{B}(-\mathbf{k}) = \mathbf{B}_\mathrm{B}(\mathbf{k}). \tag{3.38}$$

So if the system is symmetric under both time reversal and spatial inversion, then

$$\mathbf{B}_\mathrm{B}(\mathbf{k}) = -\mathbf{B}_\mathrm{B}(\mathbf{k}), \tag{3.39}$$

and we conclude that $\mathbf{B}_\mathrm{B} = \mathbf{0}$, i.e. Berry's curvature—and thereby also Berry's phase—vanish if both time-reversal symmetry and spatial inversion symmetry persist. We therefore conclude that the anomalous velocity is nonzero only if either spatial inversion symmetry or time-reversal symmetry is broken.

In summary, the anomalous velocity comes from Berry's connection in Eq. (3.23), which is included in the wave packet describing the system, such that the wave packet in Eq. (3.20) is always centered at a specific position. This 'extra' velocity is to be included in the description of the dynamics of the system, when either time-reversal or spatial inversion symmetry is broken. The breaking of inversion symmetry happens exactly at the surface of a metal and since the transport contributing states of topological insulators are the surface states, the effects of Berry's curvature is necessary for a complete description of the electron dynamics [15].

3.2 Berry's phase in mass-gapped helical systems

In this section we will investigate Berry's phase in topological insulators with a mass-induced gap. The motivation for including a mass term in the Hamiltonian is that is resembles the effect of a magnetic-field splitting, but is easier to operate with since we do not take the coupling of the momentum and magnetic field into account. First we examine if a mass term could induce a Berry phase in the low-energy regime, i.e. working with Dirac electrons, and later on we shall see what effect the inclusion of warping has on Berry's phase.

3.2.1 Berry's phase for mass-gapped Dirac spectrum

We now consider a Dirac electron system described by the Rashba Hamiltonian, and in addition we include possibility of the surface bands to be split by a mass term Δ,

$$H = \varepsilon_{\mathrm{D}}\tau_0 + \hbar v_{\mathrm{F}}(k_y\tau_x - k_x\tau_y) + \Delta\tau_z, \tag{3.40}$$

in which the electron energy spectrum are

$$E_{\pm}(k) = \varepsilon_{\mathrm{D}} \pm \sqrt{\Delta^2 + (\hbar v_{\mathrm{F}}k)^2} \equiv \varepsilon_{\mathrm{D}} \pm \sqrt{\Delta^2 + \varepsilon_k^2}. \tag{3.41}$$

The eigenspinors of this Hamiltonian describing a positive (+) or negative (−) helicity electron are in Sec. A.3 listed as

$$\chi_{\pm}(\mathbf{k}) = \frac{1}{\sqrt{2}}\begin{pmatrix} u_{\pm}(\mathbf{k})\,\mathrm{e}^{\mathrm{i}\arg(\mathrm{i}k_-)} \\ \pm u_{\mp}(\mathbf{k}) \end{pmatrix} = \frac{1}{\sqrt{2}}\begin{pmatrix} u_{\pm}(\mathbf{k})\,\mathrm{e}^{-\mathrm{i}\theta(\mathbf{k})} \\ \pm u_{\mp}(\mathbf{k}) \end{pmatrix}, \tag{3.42}$$

where the directional angle is

$$\arg(\mathrm{i}k_-) = \arctan\left(\frac{k_x}{k_y}\right) \equiv -\theta(\mathbf{k}), \tag{3.43}$$

and the coefficients associated with the mass term is

$$u_{\pm}(\mathbf{k}) = \sqrt{1 \pm \frac{\Delta}{\sqrt{\Delta^2 + (\hbar v_{\mathrm{F}}k)^2}}} = \sqrt{1 + \frac{\Delta}{E_{\pm}(\mathbf{k}) - \varepsilon_{\mathrm{D}}}}, \tag{3.44}$$

where the second equality follows from Eq. (3.41).

Using the eigenspinors of the system, Berry's curvature in Eq. (3.17) becomes

$$\begin{aligned}
\mathbf{A}_{\mathrm{B},\pm}(\mathbf{k}) &= \mathrm{i}\chi_{\pm}^{\dagger}\partial_{\mathbf{k}}\chi_{\pm} \\
&= \frac{\mathrm{i}}{2}\begin{pmatrix} u_{\pm}^*\,\mathrm{e}^{\mathrm{i}\theta} & \pm u_{\mp}^* \end{pmatrix}\begin{pmatrix} (\partial_{\mathbf{k}}u_{\pm} - \mathrm{i}u_{\pm}\partial_{\mathbf{k}}\theta)\,\mathrm{e}^{-\mathrm{i}\theta} \\ \pm\partial_{\mathbf{k}}u_{\mp} \end{pmatrix} \\
&= \frac{\mathrm{i}}{2}(-\mathrm{i}|u_{\pm}|^2\partial_{\mathbf{k}}\theta + u_{\pm}^*\partial_{\mathbf{k}}u_{\pm} + u_{\mp}^*\partial_{\mathbf{k}}u_{\mp}), \\
&= \frac{1}{2}|u_{\pm}(\mathbf{k})|^2\partial_{\mathbf{k}}\theta(\mathbf{k}),
\end{aligned} \tag{3.45}$$

since with $z(k) \equiv \Delta/\sqrt{\Delta^2 + \varepsilon_k^2}$,

$$\partial_{\mathbf{k}}u_{\pm}(k) = \partial_{\mathbf{k}}\sqrt{1 \pm z(k)} = \frac{1}{2\sqrt{1 \pm z(k)}}\partial_{\mathbf{k}}\big(1 \pm z(k)\big) = \pm\frac{1}{2u_{\pm}(k)}\partial_{\mathbf{k}}z(k), \tag{3.46}$$

which means that since $u_{\pm}$ is always a real, positive quantity,

$$u_{\pm}^*(k)\partial_{\mathbf{k}}u_{\pm}(k) = u_{\pm}(k)\partial_{\mathbf{k}}u_{\pm}(k) = \pm\frac{1}{2}\partial_{\mathbf{k}}z(k), \tag{3.47}$$

and, for general expressions of $u_{\pm}$, we have that $u_+^*\partial_{\mathbf{k}}u_+$ and $u_-^*\partial_{\mathbf{k}}u_-$ cancel each other. Furthermore, only the z component of Berry's curvature yields something nonzero, namely

$$\begin{aligned}
B_{\mathrm{B},\pm,z}(\mathbf{k}) &= [\partial_{\mathbf{r}} \times \mathbf{A}_{\mathrm{B},\pm}]_z \\
&= \partial_{k_x}A_{\mathrm{B},y} - \partial_{k_y}A_{\mathrm{B},x} \\
&= \frac{1}{2}\Big[(\partial_{k_x}|u_{\pm}(k)|^2)\partial_{k_y}\theta(\mathbf{k}) - (\partial_{k_y}|u_{\pm}(k)|^2)\partial_{k_x}\theta(\mathbf{k})\Big].
\end{aligned} \tag{3.48}$$

Realizing that

$$\partial_{k_\alpha}|u_\pm(k)|^2 = \partial_{k_\alpha}u_\pm^2 = \mp\frac{2(\hbar v)^2\Delta}{(\sqrt{\Delta^2+\varepsilon_k^2})^3}k_\alpha, \tag{3.49}$$

Berry's curvature becomes

$$\mathbf{B}_{\mathrm{B},\pm}(\mathbf{k}) = \mp\frac{(\hbar v_\mathrm{F})^2\Delta}{2(\sqrt{\Delta^2+\varepsilon_k^2})^3}\big(k_x\partial_{k_y}\theta - k_y\partial_{k_x}\theta\big)\hat{\mathbf{z}}. \tag{3.50}$$

From Eq. (3.43) we obtain

$$\partial_{k_x}\theta(\mathbf{k}) = -\frac{k_y}{k^2}, \tag{3.51}$$

$$\partial_{k_y}\theta(\mathbf{k}) = \frac{k_x}{k^2}, \tag{3.52}$$

so that

$$\mathbf{B}_{\mathrm{B},\pm}(\mathbf{k}) = \mp\frac{(\hbar v)^2\Delta}{(E_\pm(k)-\varepsilon_\mathrm{D})^3}\hat{\mathbf{z}}. \tag{3.53}$$

Berry's connection is given by combining

$$|u_\pm(k)|^2 = 1 \pm \frac{\Delta}{\sqrt{\Delta^2+\varepsilon_k^2}} = 1 + \frac{\Delta}{E_\pm(k)-\varepsilon_\mathrm{D}}, \tag{3.54}$$

with Eqs. (3.51) and (3.52) into Eq. (3.45), so that

$$\mathbf{A}_{\mathrm{B},\pm}(\mathbf{k}) = \frac{1}{2}\left(1+\frac{\Delta}{E_\pm(k)-\varepsilon_\mathrm{D}}\right)\frac{1}{k^2}\begin{pmatrix}-k_y\\ k_x\end{pmatrix}, \tag{3.55}$$

so Berry's phase is

$$\begin{aligned}\gamma_{\mathrm{B},\pm} &= \oint \mathrm{d}\mathbf{k}\cdot\mathbf{A}_{\mathrm{B},\pm}(\mathbf{k})\\ &= \int \mathrm{d}k_x\, A_{\mathrm{B},\pm,x}(\mathbf{k}) + \int \mathrm{d}k_y\, A_{\mathrm{B},\pm,y}(\mathbf{k})\\ &= -\int \mathrm{d}k_x\,\frac{1}{2}\left(1+\frac{\Delta}{E_\pm(k)-\varepsilon_\mathrm{D}}\right)\frac{1}{k^2}k_y + \int \mathrm{d}k_y\,\frac{1}{2}\left(1+\frac{\Delta}{E_\pm(k)-\varepsilon_\mathrm{D}}\right)\frac{1}{k^2}k_x.\end{aligned} \tag{3.56}$$

Using the circular parametrizations of the constant-energy contour,

$$k_x = k\cos\theta, \tag{3.57}$$

$$k_y = k\sin\theta, \tag{3.58}$$

such that we can change the wave number variable to the directional angle on the constant-energy, such that

$$\mathrm{d}k_x = -\mathrm{d}\theta\, k\sin\theta, \tag{3.59}$$

$$\mathrm{d}k_y = \mathrm{d}\theta\, k\cos\theta, \tag{3.60}$$

yields a Berry phase of

$$\begin{aligned}\gamma_{\mathrm{B},\pm} = &\int_0^{2\pi}(-\mathrm{d}\theta\, k\sin\theta)\left[-\frac{1}{2}\left(1+\frac{\Delta}{E_\pm(k)-\varepsilon_\mathrm{D}}\right)\right]\frac{k\sin\theta}{k^2}\\ &+\int_0^{2\pi}(\mathrm{d}\theta\, k\cos\theta)\left[\frac{1}{2}\left(1+\frac{\Delta}{E_\pm(k)-\varepsilon_\mathrm{D}}\right)\right]\frac{k\cos\theta}{k^2},\end{aligned} \tag{3.61}$$

which evaluates to

$$\gamma_{\mathrm{B},\pm} = \pi\left(1+\frac{\Delta}{E_\pm(\mathbf{k})-\varepsilon_\mathrm{D}}\right), \tag{3.62}$$

or

$$\gamma_{\mathrm{B},\pm} = \pi\left(1\pm\frac{\Delta}{\sqrt{\Delta^2+\varepsilon_k^2}}\right). \tag{3.63}$$

Since

$$\mathrm{e}^{\mathrm{i}(\gamma_\pm+n2\pi)} = \mathrm{e}^{\mathrm{i}\gamma_\pm}, \qquad n\in\mathbb{Z}, \tag{3.64}$$

we are free to substract 2π from the original positive-helicity Berry phase, so

$$\gamma_{\mathrm{B},+} = \pi\left(1 + \frac{\Delta}{\sqrt{\Delta^2 + \varepsilon_k^2}}\right) - 2\pi = -\pi\left(1 - \frac{\Delta}{\sqrt{\Delta^2 + \varepsilon_k^2}}\right), \tag{3.65}$$

such that Berry's phase is defined in the intervals,

$$-\pi < \gamma_{\mathrm{B},+} < 0, \tag{3.66}$$

$$0 < \gamma_{\mathrm{B},-} < \pi, \tag{3.67}$$

and therefore

$$\gamma_{\mathrm{B},\pm} = \mp\pi\left(1 - \frac{\Delta}{\sqrt{\Delta^2 + \varepsilon_k^2}}\right). \tag{3.68}$$

Thus we see that a Dirac electron can only have a nonzero Berry phase if the electron energy spectrum is gapped by a mass-like term, $\Delta\tau_z$. This is also derived in [14]. For massless Dirac electrons, Berry's phase in Eq. (3.68) becomes

$$\gamma_{\mathrm{B},\pm} \to \mp\pi \qquad \text{for} \qquad \Delta \to 0, \tag{3.69}$$

which is just the phase a Dirac electron picks up due to spin–momentum locking after a complete rotation around in the Brillouin zone. This contribution of π is what [16] calls the topological phase. This naming is motivated by the fact that this contribution exist purely due to the topological surface states and not due to external effects, such as the mass term in the system considered above. All other effects are gathered in the nontopological term, which in the above case is the second term in Eq. (3.68).

Because of the mass-gap dependence in Eq. (3.53), Berry's curvature is only nonzero if $\Delta \neq 0$. Hence the anomalous velocity will also vanish. This is verified by using the no-gapped eigenspinors,

$$\chi_\pm(\mathbf{k}) = \frac{1}{\sqrt{2}}\begin{pmatrix} \mathrm{e}^{-\mathrm{i}\theta(\mathbf{k})} \\ \pm 1 \end{pmatrix}, \tag{3.70}$$

which gives a Berry connection of

$$\mathbf{A}_{\mathrm{B},\pm}(\mathbf{k}) = \mathrm{i}\chi_\pm^\dagger(\mathbf{k})\partial_{\mathbf{k}}\chi_\pm(\mathbf{k}) = \frac{1}{2}\partial_{\mathbf{k}}\theta(\mathbf{k}) = \frac{1}{2}\frac{1}{k^2}\begin{pmatrix} -k_y \\ k_x \end{pmatrix}. \tag{3.71}$$

Then

$$\mathbf{B}_{\mathrm{B},\pm}(\mathbf{k}) = \partial_{\mathbf{k}} \times \mathbf{A}_{\mathrm{B},\pm}(\mathbf{k}) = (\partial_{k_x}A_{\mathrm{B},y} - \partial_{k_y}A_{\mathrm{B},x})\hat{\mathbf{z}} = \mathbf{0}, \tag{3.72}$$

and the anomalous velocity vanish together with it,

$$\dot{\mathbf{r}}_{\mathrm{a}} = -\dot{\mathbf{k}} \times \mathbf{B}_{\mathrm{B}}(\mathbf{k}) = \mathbf{0}. \tag{3.73}$$

We therefore conclude that in the absence of some gap-inducing mechanism, such as a magnetic field or a mass term in the Hamiltonian, the anomalous velocity of the Dirac electrons is zero, and the velocity of the Dirac electron is described by the group velocity only.

3.2.2 Berry's phase for mass-gapped helical electrons with warping

We now investigate Berry's phase for the same system as in Sec. 3.2.1, but we now include the warping effects through the warping Hamiltonian

$$H_{\mathrm{W}} = 2\hbar^3\lambda\cos 3\theta k^3\tau_z = \varepsilon_{\mathrm{W}}(\mathbf{k})\tau_z, \tag{3.74}$$

with the 'warping energy' being

$$\varepsilon_{\mathrm{W}}(\mathbf{k}) \equiv 2\hbar^3\lambda\cos 3\theta k^3, \tag{3.75}$$

such that we are considering the effective Hamiltonian

$$H = \varepsilon_{\mathrm{D}}\tau_0 + \hbar v_{\mathrm{F}}(k_y\tau_x - k_x\tau_y) + \Delta\tau_z + 2\lambda\hbar^3\cos 3\theta k^3\tau_z. \tag{3.76}$$

The eigenspinors of this system are the same as in Eq. (3.42), but with the modified coefficients

$$u_\pm(\mathbf{k}) = \sqrt{1 \pm \frac{\Delta + \varepsilon_{\mathrm{W}}(\mathbf{k})}{\sqrt{\big(\Delta + \varepsilon_{\mathrm{W}}(\mathbf{k})\big)^2 + \varepsilon_k^2}}}, \tag{3.77}$$

i.e. an effective change of Δ in Eq. (3.44) into $\Delta+\varepsilon_{\mathrm{W}}$. The directional angle is still given by Eq. (3.43). Warping of the constant-energy contours introduces an angular dependence in the modulus of the wave number k leading to a nontrivial xy parametrization,

$$k_x(\theta) = k(\theta)\cos\theta, \tag{3.78}$$
$$k_y(\theta) = k(\theta)\sin\theta, \tag{3.79}$$

where the θ parametrization of the modulus of the wave vector comes from solving

$$E_{\pm}(\mathbf{k}) = \varepsilon_{\mathrm{D}} \pm \sqrt{(\Delta + 2\lambda\hbar^3\cos 3\theta k^3)^2 + (\hbar v_{\mathrm{F}})^2 k^2} = E, \tag{3.80}$$

for k, which can be done numerically. Hence k will be a function of both the 'probing energy' E and the directional angle θ. As in the previous section, Berry's phase can be expressed as

$$\gamma_{\pm} = \oint_{\mathrm{BZ}} \mathrm{d}\mathbf{k}\cdot\mathbf{A}_{\mathrm{B}}(\mathbf{k}) = \int \mathrm{d}k_x\, A_{\mathrm{B},x}(\mathbf{k}) + \int \mathrm{d}k_y\, A_{\mathrm{B},y}(\mathbf{k}). \tag{3.81}$$

As in the case of the Dirac system in the previous section, Berry's connection is still Eq. (3.55) with the aforementioned substitution, $\Delta \to \Delta + \varepsilon_{\mathrm{W}}$, since Eq. (3.45) still applies due to the argument below Eq. (3.47), so

$$\mathbf{A}_{\mathrm{B},\pm}(\mathbf{k}) = \frac{1}{2}\left(1 \pm \frac{\Delta + 2\lambda\hbar^3\cos 3\theta k^3(\theta,E)}{\sqrt{(\Delta + 2\lambda\hbar^3\cos 3\theta k^3(\theta,E))^2 + (\hbar v_{\mathrm{F}})^2 k^2(\theta,E)}}\right)\frac{1}{k^2(\theta,E)}\begin{pmatrix}-k_y(\theta,E)\\ k_x(\theta,E)\end{pmatrix}. \tag{3.82}$$

Then

$$\mathrm{d}k_x = \mathrm{d}\theta\frac{\mathrm{d}k_x}{\mathrm{d}\theta} = \mathrm{d}\theta\left(\frac{\mathrm{d}k}{\mathrm{d}\theta}\cos\theta - k(\theta)\sin\theta\right), \tag{3.83}$$
$$\mathrm{d}k_y = \mathrm{d}\theta\frac{\mathrm{d}k_y}{\mathrm{d}\theta} = \mathrm{d}\theta\left(\frac{\mathrm{d}k}{\mathrm{d}\theta}\sin\theta + k(\theta)\cos\theta\right), \tag{3.84}$$

which enables us to recast the phase in Eq. (3.81) as

$$\begin{aligned}\gamma_{\pm} = &\int_0^{2\pi}\mathrm{d}\theta\ (\partial_\theta k(\theta,E)\cos\theta - k(\theta,E))\sin\theta)\\ &\frac{1}{2}\left(1 \pm \frac{\Delta + 2\lambda\hbar^3\cos 3\theta k^3(\theta,E)}{\sqrt{(\Delta + 2\lambda\hbar^3\cos 3\theta k^3(\theta,E))^2 + (\hbar v_{\mathrm{F}})^2 k^2(\theta,E)}}\right)\left(-\frac{k(\theta,E)\sin\theta}{k^2(\theta,E)}\right)\\ &+\int_0^{2\pi}\mathrm{d}\theta\ (\partial_\theta k(\theta,E)\sin\theta + k(\theta,E)\cos\theta)\\ &\frac{1}{2}\left(1 \pm \frac{\Delta + 2\lambda\hbar^3\cos 3\theta k^3(\theta,E)}{\sqrt{(\Delta + 2\lambda\hbar^3\cos 3\theta k^3(\theta,E))^2 + (\hbar v_{\mathrm{F}})^2 k^2(\theta,E)}}\right)\left(\frac{k(\theta,E)\cos\theta}{k^2(\theta,E)}\right),\end{aligned} \tag{3.85}$$

or simply as

$$\gamma_{\pm} = \mp\frac{1}{2}\int_0^{2\pi}\mathrm{d}\theta\left(1 - \frac{\Delta + 2\lambda\hbar^3\cos 3\theta k^3(\theta,E)}{\sqrt{(\Delta + 2\lambda\hbar^3\cos 3\theta k^3(\theta,E))^2 + (\hbar v_{\mathrm{F}})^2 k^2(\theta,E)}}\right), \tag{3.86}$$

where we have used the phase argument in connection to Eq. (3.64) to shift Berry's phase so that it fulfills Eqs. (3.66) and (3.67). This integral clearly consists of two parts: The topogical part of Berry's phase, $\gamma_{\mathrm{top.},\pm} = \mp\pi$, and the other nontopological part which depends on the mass splitting and the warping. The integral is numerically evaluated using the values

$$\hbar v_{\mathrm{F}} = 3100\ \mathrm{meV\,\AA}, \tag{3.87}$$
$$\hbar^3\lambda = 10^5\ \mathrm{meV\,\AA}^3, \tag{3.88}$$
$$\varepsilon_{\mathrm{D}} = -330\ \mathrm{meV}, \tag{3.89}$$
$$\Delta = 10\ \mathrm{meV}, \tag{3.90}$$

at the Fermi surface $E_+ = \varepsilon_{\mathrm{F}} = 0$, and the result for the magnitude of Berry's phase of a warped, helical electron with positive helicity as a function of the warping strength λ is shown in the plot in Fig. 3.1. Hence the warping effect makes Berry's phase increase as the warping strength is increased.

This means that the nontopological part of Berry's phase makes a negative, warping-dependent contribution to Berry's phase. For comparison Berry's phase without warping is shown as the red line in Fig. 3.1 at the Fermi surface,

$$|\gamma_{+,\lambda=0}| = \pi \left(1 - \frac{\Delta}{E_+ - \varepsilon_{\mathrm{D}}}\right) = 3.046. \tag{3.91}$$

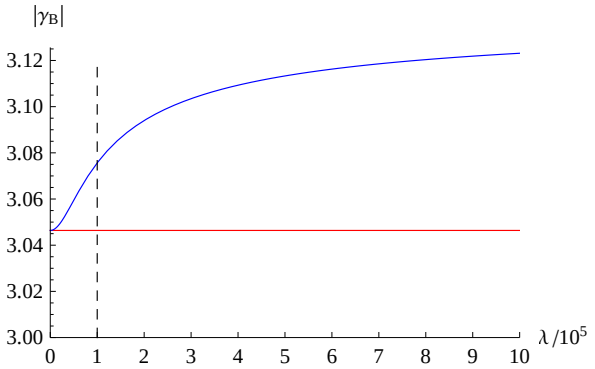

Figure 3.1: The magnitude of Berry's phase for a positive-helicity electron as a function of the warping strength (blue line) for a system described by Eq. (3.76), i.e. with warping. Also plotted is Berry's phase *without* warping (red line).

3.3 The anomalous quantum Hall conductivity

3.3.1 Quantum Hall effect from the anomalous velocity

We now go back and look at the dynamics of the Dirac electrons. As discussed in Sec. 3.1 a nonzero Berry curvature results in a nonzero anomalous velocity of the electron wave packet. This effect can give rise to an anomalous quantum Hall effect, which appears as a spontaneous Hall current in a ferromagnetic material in response to an electric field alone, i.e. no magnetic fields are needed [15]. With a nonzero purely electric field, i.e. $\mathbf{E} \neq \mathbf{0}$, but $\mathbf{B} = \mathbf{0}$, the k-space dynamics is governed by the following Lorentz force law,

$$\dot{\mathbf{k}} = -\frac{e}{\hbar}\mathbf{E}, \tag{3.92}$$

so in addition to the ordinary group velocity,

$$\dot{\mathbf{r}}_{\mathrm{g}}(\mathbf{k}) = \frac{1}{\hbar}\frac{\partial E_{\pm}}{\partial \mathbf{k}} = \frac{1}{\hbar}\frac{\hbar v_{\mathrm{F}}^2}{E_{\pm}(\mathbf{k}) - \varepsilon_{\mathrm{D}}}\mathbf{k} = -\frac{e}{\hbar}\frac{v_{\mathrm{F}}^2}{E_{\pm}(\mathbf{k}) - \varepsilon_{\mathrm{D}}}\mathbf{E}t, \tag{3.93}$$

the electron in the material hence acquires an anomalous velocity proportional to Berry's curvature $\mathbf{B}_{\mathrm{B}}$,

$$\dot{\mathbf{r}}_{\mathrm{a}}(\mathbf{k}) = -\dot{\mathbf{k}} \times \mathbf{B}_{\mathrm{B}}(\mathbf{k}) = \frac{e}{\hbar}\mathbf{E} \times \mathbf{B}_{\mathrm{B}}(\mathbf{k}). \tag{3.94}$$

In this case the anomalous velocity is always transverse to the electric field as shown in Fig. 3.2, which will give rise to the intrinsic Hall current. An electric field will shift the Fermi sea in the transverse direction leading to the intrinsic Hall current,

$$\mathbf{j}_{\mathrm{int}} = -e\sum_{\sigma}\int_{\mathrm{BZ}}\frac{\mathrm{d}\mathbf{k}}{(2\pi)^2} f(\mathbf{k})\dot{\mathbf{r}}_{\mathrm{a}}(\mathbf{k}) = -e^2\sum_{\sigma}\mathbf{E} \times \int_{\mathrm{BZ}}\frac{\mathrm{d}\mathbf{k}}{(2\pi)^2} f(\mathbf{k})\mathbf{B}_{\mathrm{B}}(\mathbf{k}), \tag{3.95}$$

where f is the electron distribution in the given band. The Hall conductivity is then,

$$\sigma_{xy} = \frac{\partial j_x^{\mathrm{int}}}{\partial E_y}, \tag{3.96}$$

and since

$$\mathbf{E} \times \mathbf{B}_{\mathrm{B}} = \begin{pmatrix} E_y B_{\mathrm{B},z} - E_z B_{\mathrm{B},y} \\ E_z B_{\mathrm{B},x} - E_x B_{\mathrm{B},z} \\ E_x B_{\mathrm{B},y} - E_y B_{\mathrm{B},x} \end{pmatrix}, \tag{3.97}$$

we have

$$\frac{\partial}{\partial E_y}(\mathbf{E} \times \mathbf{B}_{\mathrm{B}})_x = B_{\mathrm{B},z}, \tag{3.98}$$

so the intrinsic conductivity becomes

$$\sigma_{xy} = \frac{e^2}{\hbar}\int_{\mathrm{BZ}}\frac{\mathrm{d}\mathbf{k}}{(2\pi)^2} f(\mathbf{k})B_{\mathrm{B},z}. \tag{3.99}$$

Hence the Berry-phase supported anomalous velocity in Eq. (3.94) gives rise to a anomalous quantum Hall effect, which flows transverse to the applied electric field.

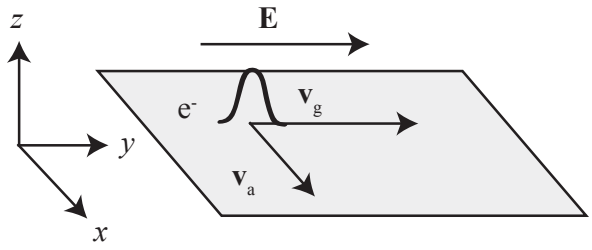

Figure 3.2: Conceptual sketch of the motion of the electron wave packet with anomalous velocity, $\mathbf{v}_{\mathrm{a}}$, and the group velocity $\mathbf{v}_{\mathrm{g}}$, with a constant, uniform electric field along the x-axis.

3.3.2 The quantum anomalous Hall conductivity

Inspired by [17] we set out to find the Hall conductivity σ_{xy}. The Rashba Hamiltonian

$$H(\mathbf{k}) = \boldsymbol{\tau} \cdot \left(\hbar v_{\mathrm{F}}(\mathbf{k} \times \hat{\mathbf{z}}) + \Delta \hat{\mathbf{z}}\right) \tag{3.100}$$

can be written on the compact form

$$H(\mathbf{k}) = \boldsymbol{\tau} \cdot \mathbf{d}(\mathbf{k}) \tag{3.101}$$

where

$$\mathbf{d}(\mathbf{k}) \equiv \hbar v_{\mathrm{F}}(\mathbf{k} \times \hat{\mathbf{z}}) + \Delta \hat{\mathbf{z}} = \begin{pmatrix} \hbar v_{\mathrm{F}} k_y \\ -\hbar v_{\mathrm{F}} k_x \\ \Delta \end{pmatrix}. \tag{3.102}$$

The corresponding unit vector is

$$\hat{\mathbf{d}}(\mathbf{k}) = \frac{1}{\sqrt{(\hbar v_{\mathrm{F}} k)^2 + \Delta^2}} \begin{pmatrix} \hbar v_{\mathrm{F}} k_y \\ -\hbar v_{\mathrm{F}} k_x \\ \Delta \end{pmatrix}. \tag{3.103}$$

This unit vector $\hat{\mathbf{d}}$ can be thought of as a mapping from the first Brillouin zone to the unit sphere S^2. A visualization of this unit vector is shown in Fig. 3.3. The Δ term opens up a gap in the band structure of the edge states as shown in Fig. 3.4.

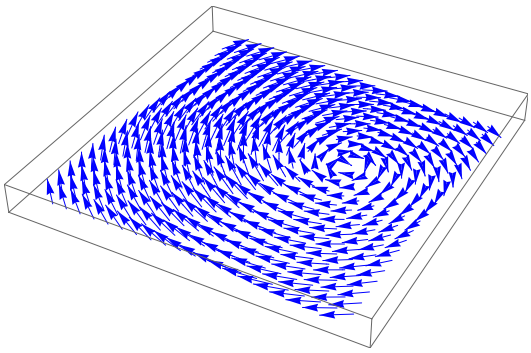

Figure 3.3: The mapping vector $\hat{\mathbf{d}}$ in the $k_x k_y$ plane.

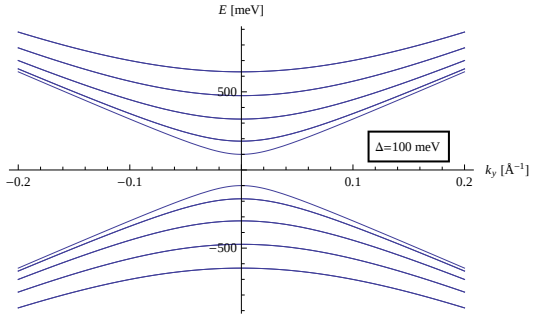

Figure 3.4: The Δ-gapped electron energy spectrum E versus k_y at various values of $-0.2\ \text{Å}^{-1} < k_x < 0.2\ \text{Å}^{-1}$.

In the case where the system becomes insulating, i.e. the chemical potential lies inside the gap of the valence band (E_-) and conduction band (E_+),

$$\min E_+(\mathbf{k}) < \mu < \max E_-(\mathbf{k}), \qquad \mathbf{k} \in \mathrm{BZ}, \tag{3.104}$$

the formula for the Hall conductivity in the continuum limit is given by [17] as

$$\sigma_{xy} = -\frac{e^2}{\hbar} \frac{1}{8\pi^2} \iint_{\mathrm{FBZ}} \mathrm{d}k_x \mathrm{d}k_y\, \hat{\mathbf{d}}(\mathbf{k}) \cdot \left(\partial_{k_x} \hat{\mathbf{d}}(\mathbf{k}) \times \partial_{k_y} \hat{\mathbf{d}}(\mathbf{k})\right), \tag{3.105}$$

where, in general, $\hat{\mathbf{d}} \cdot (\partial_{k_x} \hat{\mathbf{d}} \times \partial_{k_y} \hat{\mathbf{d}})$ is the Jacobian of the mapping $\hat{\mathbf{d}}$. In the integral in Eq. (3.105) we identify Berry's curvature, such that we can write the Hall conductivity as

$$\sigma_{xy} = -\frac{e^2}{\hbar} \frac{1}{8\pi^2} \int_{\mathrm{FBZ}} \mathrm{d}\mathbf{S}_k \cdot \mathbf{B}_{\mathrm{B}}(\mathbf{k}), \tag{3.106}$$

where $\mathrm{d}S_k$ is the surface area in k space. Furthermore, we have

$$\mathbf{B}_{\mathrm{B}}(\mathbf{k}) = \hat{\mathbf{d}} \cdot (\partial_{k_x} \hat{\mathbf{d}} \times \partial_{k_y} \hat{\mathbf{d}}) = \frac{(\hbar v_{\mathrm{F}})^2 \Delta}{\left(v_{\mathrm{F}}^2 (k_x^2 + k_y^2) + \Delta^2\right)^{3/2}}. \tag{3.107}$$

In order to obtain the Hall conductivity, we integrate Eq. (3.107) in momentum space bounded by some cut-off value, $\pm k_{\mathrm{c}}$, and since we are working in the continuum model, we can take the momentum-space boundaries to infinity, $k_{\mathrm{c}} \to \infty$, so in general,

$$\sigma_{xy} = -\frac{1}{8\pi^2} \frac{e^2}{\hbar} \lim_{k_{\mathrm{c}} \to \infty} \int_{-k_{\mathrm{c}}}^{k_{\mathrm{c}}} \mathrm{d}k_x \int_{-k_{\mathrm{c}}}^{k_{\mathrm{c}}} \mathrm{d}k_y\, \frac{v_{\mathrm{F}}^2 \Delta}{\left((\hbar v_{\mathrm{F}})^2 (k_x^2 + k_y^2) + \Delta^2\right)^{3/2}}, \tag{3.108}$$

which evaluates to

$$\sigma_{xy} = -\frac{1}{4\pi}\frac{e^2}{\hbar}. \tag{3.109}$$

This result is for the case where $\hat{\mathbf{d}}$ traverses the S^2 sphere once. If $\hat{\mathbf{d}}$ traverses the sphere n times, the k-space area calculated in Eq. (3.108) will be n times this result, i.e.

$$\sigma_{xy,n} = -\frac{n}{4\pi}\frac{e^2}{\hbar}. \tag{3.110}$$

Hence we see that the Hall conductivity for a two-dimensional insulator is quantized through $n \in \mathbb{Z}$, when the unit vector $\hat{\mathbf{d}}$ traverses the S^2 sphere n times. Since n determines how many times the mapping vector $\hat{\mathbf{d}}$, associated with the topological edge states, winds around the S^2 sphere, n is called the topological winding number.

3.3.3 Hall conductivity from a Green's function approach

Originally, Eq. (3.105) was derived in [17] using the Kubo formula,

$$Q_{xy}(\mathrm{i}q_n) = -\frac{\mathrm{i}}{\mathcal{V}}\frac{1}{\beta}\sum_{\mathrm{i}k_n,\mathbf{k}} \mathrm{Tr}\left[J_x(\mathbf{k})G(\mathbf{k},\mathrm{i}k_n+\mathrm{i}q_n)J_y(\mathbf{k})G(\mathbf{k},\mathrm{i}k_n)\right]. \tag{3.111}$$

By introducing operators,

$$P_\pm \equiv \frac{1}{2}(1 \pm \hat{d}_\alpha(\mathbf{k})\tau^\alpha), \tag{3.112}$$

one can rewrite the single-particle Matsubara Green's function as

$$\mathcal{G}(\mathbf{k},\mathrm{i}k_n) = [\hbar\mathrm{i}k_n - H(\mathbf{k})]^{-1} = \frac{P_+}{\hbar\mathrm{i}k_n - E_+(\mathbf{k})} + \frac{P_-}{\hbar\mathrm{i}k_n - E_-(\mathbf{k})}. \tag{3.113}$$

Inserting this in Eq. (3.111) and performing the Matsubara frequency sum, one obtains

$$\begin{aligned}\sigma_{xy} &= \lim_{\omega\to 0}\frac{\mathrm{i}}{\omega}Q_{xy}(\omega+\mathrm{i}\delta)\\ &= -\frac{\mathrm{i}}{\mathcal{V}}\sum_{\mathbf{k}}\frac{n_-(\mathbf{k})-n_+(\mathbf{k})}{\big(E_+(\mathbf{k})-E_-(\mathbf{k})\big)^2}\left(\mathrm{Tr}\left[J_x(\mathbf{k})P_+(\mathbf{k},\mathrm{i}k_n+\mathrm{i}q_n)J_y(\mathbf{k})P_-(\mathbf{k},\mathrm{i}k_n)\right]-\text{h.c.}\right).\end{aligned} \tag{3.114}$$

The contraction is

$$\begin{aligned}\mathrm{Tr}\left[J_x(\mathbf{k})P_+(\mathbf{k},\mathrm{i}k_n+\mathrm{i}q_n)J_y(\mathbf{k})P_-(\mathbf{k},\mathrm{i}k_n)\right] &= \mathrm{Tr}\left[(-v_\mathrm{F}\sigma_y)P_+(\mathbf{k},\mathrm{i}k_n+\mathrm{i}q_n)(v_\mathrm{F}\sigma_x)P_-(\mathbf{k},\mathrm{i}k_n)\right]\\ &= \frac{2\mathrm{i}v_\mathrm{F}^2\Delta}{\sqrt{(\hbar v_\mathrm{F}k)^2+\Delta^2}},\end{aligned} \tag{3.115}$$

and the denominator is

$$\big(E_+(\mathbf{k})-E_-(\mathbf{k})\big)^2 = (2\sqrt{(\hbar v_\mathrm{F}k)^2+\Delta^2})^2 = 4\big((v_\mathrm{F}k)^2+\Delta^2\big). \tag{3.116}$$

The Hall conductivity is then

$$\sigma_{xy} = -\frac{e^2}{\hbar}\frac{\mathrm{i}}{\mathcal{V}}\frac{1}{(2\pi)^2}\int_0^{2\pi}\mathrm{d}\theta\int_0^\infty \mathrm{d}k\,\big(n_-(\mathbf{k})-n_+(\mathbf{k})\big)k\left[\frac{2\mathrm{i}(\hbar v_\mathrm{F})^2\Delta}{\sqrt{(\hbar v_\mathrm{F}k)^2+\Delta^2}}\frac{1}{4\big((\hbar v_\mathrm{F}k)^2+\Delta^2\big)}\right], \tag{3.117}$$

and assuming that the valence band is filled, $n_-(\mathbf{k}) = 1$ and the conduction band is empty, $n_+(\mathbf{k}) = 0$, the conductivity is

$$\sigma_{xy} = -\frac{e^2}{\hbar}\frac{\mathrm{i}}{\mathcal{V}}\frac{1}{(2\pi)^2}\int_0^{2\pi}\mathrm{d}\theta\int_0^\infty \mathrm{d}k\,k\left[\frac{2\mathrm{i}v_\mathrm{F}^2\Delta}{\sqrt{(v_\mathrm{F}k)^2+\Delta^2}}\frac{1}{4\big((v_\mathrm{F}k)^2+\Delta^2\big)}\right] = \frac{1}{4\pi}\frac{e^2}{\hbar}, \tag{3.118}$$

which confirms the previous result from Eq. (3.109), except for a change of sign.

We note that in order to have a nonzero transverse conductivity we require that the parameter of the splitting mechanism, Δ, be nonzero. This is realized by starting from the mapping vector with $\Delta = 0$,

$$\hat{\mathbf{d}}(\mathbf{k}) = \frac{1}{v_\mathrm{F}\sqrt{k_x^2+k_y^2}}\begin{pmatrix}-v_\mathrm{F}k_y\\ v_\mathrm{F}k_x\\ 0\end{pmatrix}, \tag{3.119}$$

in which case the contraction in Eq. (3.115) vanishes, which eventually leads to a vanishing of the Hall conductivity, $\sigma_{xy}^{\Delta=0} = 0$.

3.4 Cyclotron orbits

In Ch. 2 we become absorbed in finding the eigenenergies of the Landau levels of a topological insulator and using is to calculate the DOS, but the electron motion was never further discussed. However, in this section we will solve the classical equations of motion for a Dirac electron, in order to get a good physical feeling of how the surface-state electrons behave. First this will be done for a Dirac electron, i.e. working in the low-energy regime, and later on the warping effect will be investigated.

3.4.1 Cyclotron motion of Dirac electrons

For the magnetic vector potential we choose the following symmetric gauge which preserves rotational invariance,

$$\mathbf{A} = \frac{1}{2}(\mathbf{B} \times \mathbf{r}), \tag{3.120}$$

which with a magnetic field $\mathbf{B} = B\hat{\mathbf{z}}$ along the z-axis becomes

$$\mathbf{A} = \begin{pmatrix} A_x \\ A_y \\ A_z \end{pmatrix} = \frac{B}{2}\begin{pmatrix} -y \\ x \\ 0 \end{pmatrix}. \tag{3.121}$$

The canonical momentum is then

$$\hbar k_x \to \hbar\kappa_x = \hbar k_x + eA_x = \hbar k_x - \frac{eB}{2}y, \tag{3.122}$$

$$\hbar k_y \to \hbar\kappa_y = \hbar k_y + eA_y = \hbar k_y + \frac{eB}{2}x. \tag{3.123}$$

Neglecting the effect of warping in the topological-insulator Hamiltonian we are left with the Rashba Hamiltonian and the Zeeman term,

$$\begin{aligned} H &= H_{\mathrm{R}} + H_{\mathrm{Z}} \\ &= \varepsilon_{\mathrm{D}}\tau_0 + \hbar v_{\mathrm{F}}\left[\left(k_y + \frac{eBx}{2\hbar}\right)\tau_x - \left(k_x - \frac{eBy}{2\hbar}\right)\tau_y\right] + \varepsilon_{\mathrm{Z}}\tau_z \\ &= \begin{pmatrix} \varepsilon_{\mathrm{D}} + \varepsilon_{\mathrm{Z}} & \hbar v_{\mathrm{F}}\left[(k_y + \mathrm{i}k_x) + \frac{eB}{2\hbar}(x - \mathrm{i}y)\right] \\ \hbar v_{\mathrm{F}}\left[(k_y - \mathrm{i}k_x) + \frac{eB}{2\hbar}(x + \mathrm{i}y)\right] & \varepsilon_{\mathrm{D}} - \varepsilon_{\mathrm{Z}} \end{pmatrix}, \end{aligned} \tag{3.124}$$

or

$$H = \begin{pmatrix} \varepsilon_{\mathrm{D}} + \varepsilon_{\mathrm{Z}} & \hbar v_{\mathrm{F}}\left[\left(k_y + \frac{eB}{2\hbar}x\right) + \mathrm{i}\left(k_x - \frac{eB}{2\hbar}y\right)\right] \\ \hbar v_{\mathrm{F}}\left[\left(k_y + \frac{eB}{2\hbar}x\right) - \mathrm{i}\left(k_x - \frac{eB}{2\hbar}y\right)\right] & \varepsilon_{\mathrm{D}} - \varepsilon_{\mathrm{Z}} \end{pmatrix}, \tag{3.125}$$

where

$$\varepsilon_{\mathrm{Z}} \equiv \frac{\mu_{\mathrm{B}}}{2}gB, \tag{3.126}$$

is the energy contribution from the Zeeman effect. The eigenenergies to H are,

$$E_{\pm}(\kappa) = \varepsilon_{\mathrm{D}} \pm \sqrt{\left(\frac{\mu_{\mathrm{B}}}{2}gB\right)^2 + (\hbar v_{\mathrm{F}}\kappa)^2} = \varepsilon_{\mathrm{D}} \pm \sqrt{\varepsilon_{\mathrm{Z}}^2 + \varepsilon_{\kappa}^2}, \tag{3.127}$$

where

$$\varepsilon_{\kappa} \equiv \hbar v_{\mathrm{F}}\kappa. \tag{3.128}$$

To find the classical cyclotron orbits we solve Hamilton's equations, which describes the classical real-space and momentum-space dynamics,

$$\dot{\mathbf{r}} = \frac{1}{\hbar}\frac{\partial E}{\partial \mathbf{k}}, \tag{3.129}$$

$$\dot{\mathbf{k}} = -\frac{1}{\hbar}\frac{\partial E}{\partial \mathbf{r}}. \tag{3.130}$$

Utilizing these equations of motion, we get

$$\dot{\mathbf{r}} = \frac{v_{\mathrm{F}}^2}{E_{\pm}(\kappa) - \varepsilon_{\mathrm{D}}}\begin{pmatrix} \hbar k_x - \frac{eB}{2}y \\ \hbar k_y + \frac{eB}{2}x \end{pmatrix}, \tag{3.131}$$

$$\dot{\mathbf{k}} = \frac{eB}{2\hbar}\frac{v_{\mathrm{F}}^2}{E_{\pm}(\kappa) - \varepsilon_{\mathrm{D}}}\begin{pmatrix} -\left(\hbar k_y + \frac{eB}{2}y\right) \\ \hbar k_x - \frac{eB}{2}x \end{pmatrix}, \tag{3.132}$$

which, as an aside, are compactly related as,

$$\dot{\mathbf{k}} = \frac{eB}{2\hbar}\tau_z \dot{\mathbf{r}}. \tag{3.133}$$

Integration with respect to time gives

$$\hbar k_x(t) = \frac{eB}{2}y(t) + \left(\hbar k_x(t_0) + \frac{eB}{2}y(t_0)\right) = \frac{eB}{2}y(t) + c_1, \tag{3.134}$$

$$\hbar k_y(t) = \frac{eB}{2}x(t) + \left(\hbar k_y(t_0) - \frac{eB}{2}x(t_0)\right) = \frac{eB}{2}x(t) + c_2, \tag{3.135}$$

where

$$c_1 \equiv \left(\hbar k_x(t_0) + \frac{eB}{2}y(t_0)\right), \tag{3.136}$$

$$c_2 \equiv \left(\hbar k_y(t_0) - \frac{eB}{2}x(t_0)\right). \tag{3.137}$$

Hamilton's equations then yield

$$\dot{x} = \pm\frac{v_{\mathrm{F}}^2}{\sqrt{\varepsilon_{\mathrm{Z}}^2 + v_{\mathrm{F}}^2[(c_1 - eBy(t))^2 + (c_2 + eBx(t))^2]}}\big(c_1 - eBy(t)\big), \tag{3.138}$$

$$\dot{y} = \pm\frac{v_{\mathrm{F}}^2}{\sqrt{\varepsilon_{\mathrm{Z}}^2 + v_{\mathrm{F}}^2[(c_1 - eBy(t))^2 + (c_2 + eBx(t))^2]}}\big(c_2 + eBx(t)\big), \tag{3.139}$$

so

$$\frac{\dot{x}}{\dot{y}} = \frac{c_1 - eBy(t)}{c_2 + eBx(t)}, \tag{3.140}$$

or

$$\frac{\mathrm{d}x}{\mathrm{d}y} = \frac{c_1 - eBy(t)}{c_2 + eBx(t)}, \tag{3.141}$$

which by separation of variables integrates to

$$c_1 x(t) + \frac{eB}{2}x^2(t) + F_1(y) = c_2 y(t) - \frac{eB}{2}y^2(t) + F_2(x), \tag{3.142}$$

where F_1 and F_2 are integration constant. Assuming these integration constants to be zero, we obtain

$$\left(x(t) + \frac{c_2}{eB}\right)^2 + \left(y(t) - \frac{c_1}{eB}\right)^2 = \frac{1}{(eB)^2}(c_1^2 + c_2^2). \tag{3.143}$$

Thus the orbits of the electrons are circular with center in $(c_2/(eB), c_1/(eB))$ with radius $(c_1^2 + c_2^2)/(eB)^2$. To get the actual position, we insert the above equation into Eq. (3.138), define $c^2 \equiv c_1^2 + c_2^2$ and get

$$\dot{x}(t) = \pm\frac{v_{\mathrm{F}}^2}{\sqrt{\varepsilon_{\mathrm{Z}}^2 (v_{\mathrm{F}}c)^2}}\sqrt{c^2 - (eBx(t) + c_2)^2}, \tag{3.144}$$

and by separating the variables,

$$\int_{x(t_0)}^{x(t)} \frac{\mathrm{d}x'}{\sqrt{c^2 - (eBx' + c_2)^2}} = \pm\int_{t_0}^{t} \mathrm{d}t' \frac{v_{\mathrm{F}}^2}{\sqrt{\varepsilon_{\mathrm{Z}}^2 + (v_{\mathrm{F}}c)^2}}. \tag{3.145}$$

Shifting integration variable to $z = c_2 + eBx'$ in the above equation and performing the integration gives us

$$\frac{1}{eB}\left[\arcsin\left(\frac{eBx(t) + c_2}{c}\right) - \arcsin\left(\frac{eBx(t_0) + c_2}{c}\right)\right] = \frac{v_{\mathrm{F}}^2}{E_{\pm}(\kappa) - \varepsilon_{\mathrm{D}}}(t - t_0). \tag{3.146}$$

Noting that both p and c are constants of motion and are only set by the initial conditions, they are de facto the same, $p = c$, and

$$x(t) = \frac{\hbar\kappa}{eB}\sin\left[\omega(t - t_0) + \phi_x\right] - \frac{c_2}{eB}, \tag{3.147}$$

and likewise for the y component of the velocity. The final result is the reduced parameterization of the orbit of Dirac electrons,

$$\frac{x(t)}{l_\kappa} = \sin\left(\pm\omega t + \phi_x\right) - l_\kappa^{-1}\left(\frac{\hbar k_y(0)}{eB} - \frac{x(0)}{2}\right), \tag{3.148}$$

$$\frac{y(t)}{l_\kappa} = -\sin\left(\pm\omega t + \phi_y\right) + l_\kappa^{-1}\left(\frac{\hbar k_x(0)}{eB} + \frac{y(0)}{2}\right), \tag{3.149}$$

where $l_\kappa \equiv \hbar\kappa/eB$ is a characteristic length set by the momentum initial conditions and the magnetic field, and

$$\phi_x \equiv \arcsin\left(\frac{\hbar k_y(0) + \frac{eB}{2}x(0)}{\hbar\kappa}\right), \tag{3.150}$$

$$\phi_y \equiv \arcsin\left(\frac{\hbar k_x(0) - \frac{eB}{2}y(0)}{\hbar\kappa}\right), \tag{3.151}$$

are some characteristic phases of the orbit, and

$$\omega_\pm \equiv \pm\frac{eBv_\mathrm{F}^2}{\sqrt{\varepsilon_\mathrm{Z}^2 + (\hbar v_\mathrm{F}\kappa)^2}} \tag{3.152}$$

is the frequency of the orbit, the so-called cyclotron frequency. From Eq. (3.127),

$$\pm\sqrt{\varepsilon_\mathrm{Z}^2 + (\hbar v_\mathrm{F}\kappa)^2} = E_\pm(\kappa) - \varepsilon_\mathrm{D}, \tag{3.153}$$

so the cyclotron frequency can also be written as

$$\omega_\pm = \frac{eBv_\mathrm{F}^2}{E_\pm(\kappa) - \varepsilon_\mathrm{D}}. \tag{3.154}$$

In order to find the corresponding motion in momentum space as done in [12], we note that the Lorentz force law for a electron in a purely magnetic field is

$$\hbar\dot{\mathbf{k}} = -e\mathbf{E} - e\dot{\mathbf{r}} \times \mathbf{B}, \tag{3.155}$$

and after integration with respect to time t, we obtain

$$\mathbf{k}(t) - \mathbf{k}(t_0) = -\frac{eB}{\hbar}\hat{\mathbf{B}} \times \big(\mathbf{r}(t) - \mathbf{r}(t_0)\big), \tag{3.156}$$

where $\mathbf{k}(t_0)$ and $\mathbf{r}(t_0)$ are the initial momentum and position, respectively. Hence it is readily seen that the momentum-space cyclotron orbits are just real-space cyclotron orbits rotated by $-\pi/2$ about the $\hat{\mathbf{B}}$-axis and scaled by $eB/\hbar$, so

$$\mathbf{k}(t) - \mathbf{k}(t_0) = \hat{\mathbf{B}}[\hat{\mathbf{B}} \cdot (\mathbf{r}(t) - \mathbf{r}(t_0))] - [\mathbf{r}(t) - \mathbf{r}(t_0)]. \tag{3.157}$$

In summary, classical physics prescribes that a Dirac electron in a uniform and constant magnetic field moves around at constant energy $E_\pm$ in a plane perpendicular to the magnetic field B, as seen by the parameterizations in Eqs. (3.148) and (3.149). If the magnetic field strength is high enough the electron will move around in a closed orbit, a so-called cyclotron orbit, in which it completes many revolutions.

3.4.2 Cyclotron motion with warping

When the warping effect is taken into account, the cyclotron orbits are modified, since the Fermi surface is being hexagonally warped. The motion in real space and momentum space is found from the Hamiltonian,

$$H = H_\mathrm{R} + H_\mathrm{Z} + H_\mathrm{W}, \tag{3.158}$$

where

$$H_\mathrm{R} = \begin{pmatrix} \varepsilon_\mathrm{D} & \hbar v_\mathrm{F}\left[\left(k_y + \frac{eB}{2\hbar}x\right) + \mathrm{i}\left(k_x - \frac{eB}{2\hbar}y\right)\right] \\ \hbar v_\mathrm{F}\left[\left(k_y + \frac{eB}{2\hbar}x\right) - \mathrm{i}\left(k_x - \frac{eB}{2\hbar}y\right)\right] & \varepsilon_\mathrm{D} \end{pmatrix}, \tag{3.159}$$

$$H_\mathrm{Z} = \frac{\mu_\mathrm{B}}{2}gB\tau_z, \tag{3.160}$$

$$H_\mathrm{W} = 2\hbar^3\lambda\left(\hbar k_x - \frac{eB}{2}y\right)\left[\left(\hbar k_x - \frac{eB}{2}y\right)^2 - 3\left(\hbar k_y + \frac{eB}{2}x\right)^2\right]\tau_z. \tag{3.161}$$

Finding the position analytically becomes too involved which is why we resort to a numerical calculation of the orbits, but still using Hamilton's equations. The resulting orbits for an positive-helicicty electron in a magnetic field of $B = 11$ T, experiencing a warping strength of $\hbar^3\lambda = 10^5$ meV Å^3 are shown in Figs. 3.5 and 3.6, with initial conditions $\mathbf{r} = (0, 0)$ and $k \approx 0.0927$ Å^{-1}, giving an energy close to the Fermi energy, $E \approx \varepsilon_{\mathrm{F}} = 0$. From these plots we see that the electron simply moves at the edge of the hexagonally warped Fermi surface in momentum space. The real-space motion is as previously mentioned just a scaled and rotated version of the corresponding momentum-space electron trajectories.

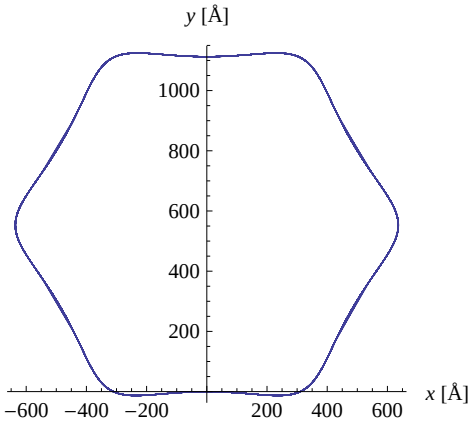

Figure 3.5: Motion of Dirac electron in real space in $B = 11$ T and $\hbar^3\lambda = 10^5$ meV Å^3 at $E \approx 0$.

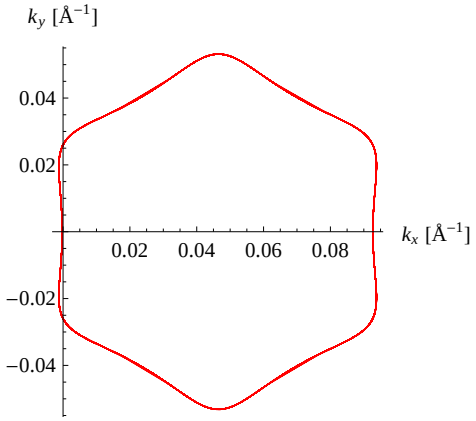

Figure 3.6: Motion of Dirac electron in momentum space in $B = 11$ T and $\hbar^3\lambda = 10^5$ meV Å^3 close to the Fermi surface.

3.5 Berry's phase in topological insulators

As mentioned in Sec. 3.2 a mass term in the Hamiltonian could open up a gap in the band energy of the surface-state electrons. Another mechanism which could open a gap is an external magnetic field. This is investigated in this section.

3.5.1 Eigenspinors

In order to find Berry's phase in the presence of an external magnetic field, we will start out by finding the eigenspinors of our system in consideration, namely a helical electron in a magnetic field B described by the Hamiltonian,

$$H = \begin{pmatrix} \varepsilon_{\mathrm{D}} + \varepsilon_{\mathrm{Z}} & \hbar v_{\mathrm{F}}(\kappa_y + \mathrm{i}\kappa_x) \\ \hbar v_{\mathrm{F}}(\kappa_y - \mathrm{i}\kappa_x) & \varepsilon_{\mathrm{D}} - \varepsilon_{\mathrm{Z}} \end{pmatrix}, \tag{3.162}$$

where

$$\kappa_x = k_x - \frac{eB}{2\hbar} y, \tag{3.163}$$

$$\kappa_y = k_y + \frac{eB}{2\hbar} x, \tag{3.164}$$

are the canonical momenta. The eigenspinors of this Hamiltonian describing a positive (+) or negative (−) helicity electron are found to be

$$\chi_{\pm}(\boldsymbol{\kappa}, t) = \frac{1}{\sqrt{2}} \begin{pmatrix} u_{\pm}(\kappa)\, \mathrm{e}^{\mathrm{i}\arg\left(\mathrm{i}\kappa_-(t)\right)} \\ \pm u_{\mp}(\kappa) \end{pmatrix}, \tag{3.165}$$

where

$$u_{\pm}(\kappa) = \sqrt{1 \pm \frac{\varepsilon_{\mathrm{Z}}}{\sqrt{\varepsilon_{\mathrm{Z}}^2 + (\hbar v_{\mathrm{F}}\kappa)^2}}} = \sqrt{1 + \frac{\varepsilon_{\mathrm{Z}}}{E_{\pm}(\kappa) - \varepsilon_{\mathrm{D}}}}, \tag{3.166}$$

where the second equality follows from Eq. (3.153), and

$$\arg(\mathrm{i}\kappa_-(t)) = \arctan\left(\frac{\hbar k_x - \frac{eB}{2} y}{\hbar k_y + \frac{eB}{2} x}\right). \tag{3.167}$$

The energy is constant so

$$\left(\hbar k_y + \frac{eB}{2} x\right)^2 + \left(\hbar k_x - \frac{eB}{2} y\right)^2 = \frac{\left(E_{\pm}(\kappa) - \varepsilon_{\mathrm{D}}\right)^2 - \varepsilon_{\mathrm{Z}}^2}{v_{\mathrm{F}}^2}, \tag{3.168}$$

which is the circle equation, so

$$\cos\theta(\kappa, t) = \pm \frac{\hbar v_{\mathrm{F}} \kappa_y}{\sqrt{(E_{\pm}(\kappa) - \varepsilon_{\mathrm{D}})^2 - \varepsilon_{\mathrm{Z}}^2}}, \tag{3.169}$$

$$\sin\theta(\kappa, t) = \mp \frac{\hbar v_{\mathrm{F}} \kappa_x}{\sqrt{(E_{\pm}(\kappa) - \varepsilon_{\mathrm{D}})^2 - \varepsilon_{\mathrm{Z}}^2}}. \tag{3.170}$$

Comparing

$$\frac{\mathrm{d}}{\mathrm{d}t}\cos\theta(\kappa, t) = \frac{\mathrm{d}\cos\theta}{\mathrm{d}\theta}\frac{\mathrm{d}\theta}{\mathrm{d}t} = \mp \sin\theta \frac{\mathrm{d}\theta}{\mathrm{d}t}, \tag{3.171}$$

with

$$\begin{aligned} \frac{\mathrm{d}}{\mathrm{d}t}\cos\theta(\kappa, t) &= \frac{\mathrm{d}}{\mathrm{d}t}\left[\pm \frac{\hbar v_{\mathrm{F}} \kappa_y}{\sqrt{(E_{\pm}(\kappa) - \varepsilon_{\mathrm{D}})^2 - \varepsilon_{\mathrm{Z}}^2}}\right] \\ &= \frac{\hbar v_{\mathrm{F}} \kappa_x}{\sqrt{(E_{\pm}(\kappa) - \varepsilon_{\mathrm{D}})^2 - \varepsilon_{\mathrm{Z}}^2}} \frac{eB v_{\mathrm{F}}^2}{E_{\pm}(\kappa) - \varepsilon_{\mathrm{D}}} \\ &= \mp \sin\theta \frac{eB v_{\mathrm{F}}^2}{E_{\pm}(\kappa) - \varepsilon_{\mathrm{D}}}, \end{aligned} \tag{3.172}$$

yields

$$\frac{\mathrm{d}}{\mathrm{d}t}\theta(\kappa, t) = \frac{eB v_{\mathrm{F}}^2}{E_{\pm}(\kappa) - \varepsilon_{\mathrm{D}}} \equiv \omega_{\pm}. \tag{3.173}$$

The angle is then

$$\theta(\kappa, t) = \omega_{\pm}(\kappa)t + \theta_0, \tag{3.174}$$

so

$$\arg\big(\mathrm{i}\kappa_-(t)\big) = \mathrm{i}\arctan\left(\frac{\kappa_x}{\kappa_y}\right) = -\mathrm{i}\theta(\kappa, t) = -\mathrm{i}\big(\omega_{\pm}(\kappa)t + \theta_0\big). \tag{3.175}$$

Choosing $\theta_0 = 0$, the eigenspinors are then

$$\chi_{\pm}(\kappa, t) = \frac{1}{\sqrt{2}}\begin{pmatrix} u_{\pm}(\kappa)\,\mathrm{e}^{-\mathrm{i}\omega_{\pm}(\kappa)t} \\ \pm u_{\mp}(\kappa) \end{pmatrix}. \tag{3.176}$$

3.5.2 Berry's phase for Dirac electrons

In this section we will investigate the geometric phase for a surface-state electron when it traverses a closed loop trajectory under the influence of a constant magnetic field. The eigenstates in the expression for the geometric phase in Eq. (3.6) is in our case the eigenspinors in Eq. (3.176), thus the expression becomes

$$\gamma_{\pm}(t) = \mathrm{i}\int_0^t \mathrm{d}t'\,\chi_{\pm}^{\dagger}(\kappa, t')\partial_{t'}\chi_{\pm}(\kappa, t'). \tag{3.177}$$

In calculating the geometric phase we need the time derivative of the eigenspinor in Eq. (3.176),

$$\partial_t\chi_{\pm}(\kappa, t) = \frac{1}{\sqrt{2}}\begin{pmatrix} u_{\pm}(\kappa)(-\mathrm{i})\omega_{\pm}(\kappa)\,\mathrm{e}^{-\mathrm{i}\omega_{\pm}(\kappa)t} \\ 0 \end{pmatrix}, \tag{3.178}$$

so that

$$\chi_{+}^{\dagger}(\kappa, t)\,\partial_t\chi_{+}(\kappa, t) = -\frac{\mathrm{i}}{2}|u_{\pm}(\kappa)|^2\omega_{\pm}(\kappa). \tag{3.179}$$

The geometric phase becomes

$$\gamma_{\pm}(t) = \mathrm{i}\int_0^t \mathrm{d}t'\,\chi_{\pm}(\boldsymbol{\kappa}, t')\partial_{t'}\chi_{\pm}(\boldsymbol{\kappa}, t') = \mathrm{i}\int_0^t \mathrm{d}t'\,\left(-\frac{\mathrm{i}}{2}\right)\left(1 + \frac{\varepsilon_{\mathrm{Z}}}{E_{\pm}(\kappa) - \varepsilon_{\mathrm{D}}}\right)\omega_{\pm}(\kappa)t. \tag{3.180}$$

Berry's phase is the geometric phase accumulated over one period, so $t = T = 2\pi/\omega_{\pm}$, and so Berry's phase for a Dirac electron with helicity $\eta = \pm$ is

$$\gamma_{\mathrm{B},\pm} = \pi\left(1 + \frac{\varepsilon_{\mathrm{Z}}}{E_{\pm}(\kappa) - \varepsilon_{\mathrm{D}}}\right), \tag{3.181}$$

or, using Eq. (3.153),

$$\gamma_{\mathrm{B},\pm} = \pi\left(1 \pm \frac{\varepsilon_{\mathrm{Z}}}{\sqrt{\varepsilon_{\mathrm{Z}}^2 + \varepsilon_{\kappa}^2}}\right). \tag{3.182}$$

Following the same line of thoughts as in Sec. 3.2, Berry's phase becomes

$$\gamma_{\mathrm{B},\pm} = \mp\pi\left(1 - \frac{\varepsilon_{\mathrm{Z}}}{\sqrt{\varepsilon_{\mathrm{Z}}^2 + \varepsilon_{\kappa}^2}}\right). \tag{3.183}$$

This is the same result as the one obtained with a mass term instead of a magnetic field term in Eq. (3.68). Turning off the magnetic field, $\varepsilon_{\mathrm{Z}} \sim B = 0$, Berry's phase becomes $\gamma_{\pm} = \mp\pi$, which corresponds to the phase which the electron picks up upon enclosing a trajectory around in the Brillouin zone. The spin of a Dirac electron lies in the xy plane only but is rotated along with the momentum vector due to the spin–momentum locking. Hence the Zeeman energy in Eq. (3.183) and the mass in Eq. (3.68) have the same physical role, namely that it adds a contribution to Berry's phase given as the ratio of the characteristic energy (Zeeman or mass) and the electron's Dirac-point-shifted band energy $E_{\pm} - \varepsilon_{\mathrm{D}}$. The other limit, i.e. when the magnetic field becomes very large, the electron spin will align in the field direction, so $\gamma_{\mathrm{B},\pm} = 0$. In summary,

$$\gamma_{\mathrm{B},\pm} \to \begin{cases} \mp\pi, & \varepsilon_{\mathrm{Z}} \ll \varepsilon_{\kappa}, \\ 0, & \varepsilon_{\mathrm{Z}} \gg \varepsilon_{\kappa}. \end{cases} \tag{3.184}$$

3.5.3 Berry's phase from the solid angle

It is quite instructive to investigate how the spin of the Dirac electrons behave when the magnetic field strength B is changed. As seen above, when an electron is taken around in a magnetic field, its wave function acquires an additional phase, Berry's phase, and this can de facto be related to the solid angle constituted by the electron's expected spin vector $\langle \boldsymbol{\tau} \rangle$. The solid angle is defined as

$$\Omega \equiv \int \mathrm{d}S \, \frac{\mathbf{r} \cdot \hat{\mathbf{n}}}{r^2}, \tag{3.185}$$

where $\mathbf{r}$ is the position vector from a reference point to an infinitesimal surface area $\mathrm{d}S$ to which $\hat{\mathbf{n}}$ is a vector normal. For a sphere the solid angle is

$$\Omega = \int_0^{2\pi} \mathrm{d}\phi \int_0^{\theta} \mathrm{d}\theta' \, \sin\theta' r^2 \frac{1}{r^2} = 2\pi(1 - \cos\theta), \tag{3.186}$$

where θ is the polar angle, which is the angle between the z-axis and the expectation value of the spin vector [10]. See Fig. 3.7. Using the eigenspinor in Eq. (3.165), the expectation value of the spin is

$$\langle \boldsymbol{\tau} \rangle \equiv \begin{pmatrix} \langle \chi_\pm | \tau_x | \chi_\pm \rangle \\ \langle \chi_\pm | \tau_y | \chi_\pm \rangle \\ \langle \chi_\pm | \tau_z | \chi_\pm \rangle \end{pmatrix} = \begin{pmatrix} \mp\sqrt{1 - \left(\frac{\varepsilon_\mathrm{Z}}{\sqrt{\varepsilon_\mathrm{Z}^2 + \varepsilon_\kappa^2}} \right)^2} \cos\phi \\ \mp\sqrt{1 - \left(\frac{\varepsilon_\mathrm{Z}}{\sqrt{\varepsilon_\mathrm{Z}^2 + \varepsilon_\kappa^2}} \right)^2} \sin\phi \\ \pm \frac{\varepsilon_\mathrm{Z}}{\sqrt{\varepsilon_\mathrm{Z}^2 + \varepsilon_\kappa^2}} \end{pmatrix}. \tag{3.187}$$

Focusing on the positive helicity states, the result in Eq. (3.187) means that when the magnetic field is turned off, the Zeeman term vanishes with it, and the projection of the spin vector onto the z-axis becomes zero. This case corresponds to the electron moving only in the xy plane. In the other limit, when the Zeeman energy becomes very large, $\varepsilon_\mathrm{Z} \gg \varepsilon_\kappa$, the x and y components of the expected spin vector vanish, whereas the z component goes to ± 1. This limit corresponds to the case where the external magnetic field is so strong that the Zeeman contribution dominates completely and the electron system then has the eigenstates of spin-up $(1, 0)$ and spin-down $(0, 1)$, corresponding to the expected spin,

$$\langle \tau_z \rangle = \pm 1. \tag{3.188}$$

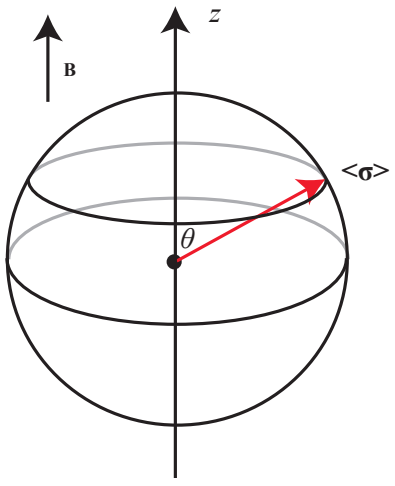

Figure 3.7: Sketch of the spin system considered in Eq. (3.187).

The projection of the spin vector onto the z-axis is

$$\langle \tau_z \rangle = \cos\theta |\langle \boldsymbol{\tau} \rangle| = \cos\theta, \tag{3.189}$$

so the solid angle simply becomes

$$\Omega_\pm = 2\pi \left[1 \mp \frac{\varepsilon_\mathrm{Z}}{\sqrt{\varepsilon_\mathrm{Z}^2 + \varepsilon_\kappa^2}} \right], \tag{3.190}$$

The relation between the solid angle and Berry's phase is [10],

$$\gamma_{\pm}(T) = \mp\frac{\Omega_{\pm}}{2}, \tag{3.191}$$

and hence Berry's phase for a positive/negative helicity Dirac electron is

$$\gamma_{\pm}(T) = \mp\pi\left[1 \mp \frac{\varepsilon_{\mathrm{Z}}}{\sqrt{\varepsilon_{\mathrm{Z}}^2 + \varepsilon_{\kappa}^2}}\right]. \tag{3.192}$$

Thus we obtain the same result as in Eq. (3.183), but by a purely geometric consideration involving the expected spin components.

The path traced out by the expected spin vector, $\langle \boldsymbol{\tau} \rangle$, with the warping effect included is shown in Fig. 3.8. The solution is obtain numerically by solving Hamilton's equations of motion, and the code used to generate this solution is found in Sec. A.4.

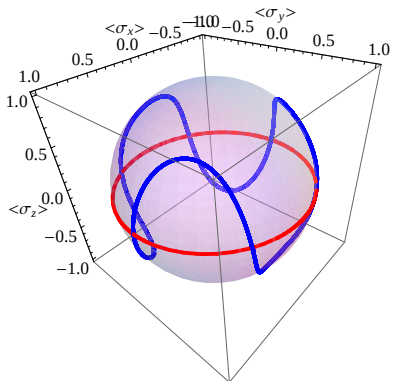

Figure 3.8: The blue curve indicates the path traced out by the expected spin vector after a complete cycle in a moderate magnetic field $B = 11$ T. The red curve indicates the Equator of the sphere.

We notice that for high field strengths, the trajectory does not precess all the way around the spin sphere but is rather localized on one side as depicted in Fig. 3.9 with warping of $\hbar^3\lambda = 10^5$ meV Å and Fig. 3.10 without warping. Both fields are at $B = 2$ kT. For such a high magnetic field the expected spin vector is strongly aligned along the z-axis in absence of warping.

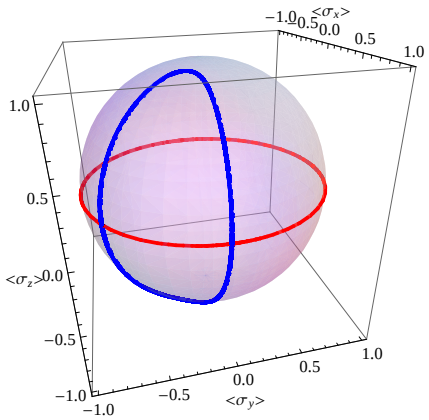

Figure 3.9: The blue curve indicates the path traced out by the expected warped spin vector after a complete cycle in high magnetic field.

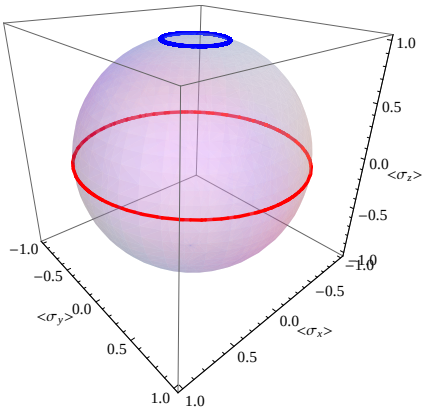

Figure 3.10: The blue curve indicates the path traced out by the expected spin vector after a complete cycle in high magnetic field *without* warping.

3.6 Quantization of semiclassical dynamics

3.6.1 The Bohr–Sommerfeld quantization condition

The Bohr–Sommerfeld quantization condition determines the approximate energies E_n of the time-independent Schrödinger equation, $H\psi_n = E_n\psi_n$. The approximation is only good if the radius of the electron trajectory r is always much larger than the lattice constant of the crystal a being considered, i.e. $r \gg a$ [18]. The Bohr–Sommerfeld quantization condition reads in general,

$$2\pi\hbar(n+\nu) = \oint \sum_i \mathrm{d}Q_i\, P_i, \tag{3.193}$$

where $n = 0, 1, 2, \ldots$ is a quantum number (which is assumed to be large), Q_i is the generalized coordinate, P_i is the generalized momentum to Q_i and ν is the Maslov index [12, 13]. In our case there are two sets of conjugate variables, namely one for the real-space coordinate, $\mathbf{r}$, and one for the momentum-space coordinate, $\mathbf{k}$, such that their canonical momenta are

$$\boldsymbol{\pi} = \frac{\partial \mathcal{L}}{\partial \dot{\mathbf{r}}} = \hbar\mathbf{k} - e\mathbf{A}(\mathbf{r}), \tag{3.194}$$

$$\mathbf{P} = \frac{\partial \mathcal{L}}{\partial \dot{\mathbf{k}}} = \hbar\mathbf{A}_{\mathrm{B}}(\mathbf{k}), \tag{3.195}$$

by using the Lagrangian in Eq. (3.32). Then Eq. (3.193) becomes

$$\begin{aligned} 2\pi\hbar(n+\nu) &= \oint \sum_i \mathrm{d}Q_i\, P_i \\ &= \oint \mathrm{d}\mathbf{k}\cdot\mathbf{P} + \oint \mathrm{d}\mathbf{r}\cdot\boldsymbol{\pi} \\ &= \hbar\oint \mathrm{d}\mathbf{k}\cdot\mathbf{A}_{\mathrm{B}} + \oint \mathrm{d}\mathbf{r}\cdot\boldsymbol{\pi} \end{aligned} \tag{3.196}$$

We recognize the first integral Eq. (3.196) as Berry's phase contribution,

$$\gamma_{\mathrm{B}} = \oint \mathrm{d}\mathbf{k}\cdot\mathbf{A}_{\mathrm{B}}, \tag{3.197}$$

to the energy quantization condition. Hence we see that Berry's phase modifies the semiclassical quantization condition for the electron energy in a magnetic field. Then

$$\oint \mathrm{d}\mathbf{r}\cdot\boldsymbol{\pi} = 2\pi\hbar\left(n+\nu-\frac{\gamma_{\mathrm{B}}}{2\pi}\right). \tag{3.198}$$

Using a symmetric gauge in which the magnetic vector potential is

$$\mathbf{A} = \frac{1}{2}\mathbf{B}\times\mathbf{r}, \tag{3.199}$$

we have that

$$\dot{\mathbf{A}} = \frac{1}{2}\mathbf{B}\times\dot{\mathbf{r}} = \frac{\hbar}{e}\dot{\mathbf{k}}, \tag{3.200}$$

by Lorentz' force law, and then by integration

$$\mathbf{A} = \frac{\hbar}{2e}\mathbf{k}. \tag{3.201}$$

The canonical momentum in Eq. (3.194) is then

$$\boldsymbol{\pi} = \hbar\mathbf{k} - e\mathbf{A} = \frac{\hbar}{2e}\mathbf{k}. \tag{3.202}$$

From Eq. (3.157) it is clear that with $l_B \equiv \sqrt{\hbar/eB}$,

$$\mathrm{d}\mathbf{r} = -l_B^2\hat{\mathbf{B}}\times\mathrm{d}\mathbf{k}, \tag{3.203}$$

and then

$$\oint \mathrm{d}\mathbf{r}\cdot\boldsymbol{\pi} = -\frac{\hbar}{2}l_B^2\hat{\mathbf{B}}\cdot\oint \mathrm{d}\mathbf{k}\times\mathbf{k}, \tag{3.204}$$

and Eq. (3.198) becomes

$$-\frac{\hbar}{2}l_B^2\hat{\mathbf{B}}\cdot\oint \mathrm{d}\mathbf{k}\times\mathbf{k} = 2\pi\hbar\left(n+\nu-\frac{\gamma_\mathrm{B}}{2\pi}\right), \tag{3.205}$$

which can be recast into

$$-\frac{1}{2}\hat{\mathbf{B}}\cdot\oint \mathrm{d}\mathbf{k}\times\mathbf{k} = 2\pi\frac{eB}{\hbar}\left(n+\nu-\frac{\gamma_\mathrm{B}}{2\pi}\right), \tag{3.206}$$

which is known as the Einstein–Keller–Brillouin quantization condition [15]. Realizing that the left side of the above equation is nothing but the k-space area enclosed at a certain energy, we obtain Onsager's quantization condition [19],

$$A_n \equiv \int \mathrm{d}\mathbf{k} = 2\pi\frac{eB}{\hbar}\left(n+\nu-\frac{\gamma_\mathrm{B}}{2\pi}\right) = 2\pi l_B^{-2}\left(n+\nu-\frac{\gamma_\mathrm{B}}{2\pi}\right). \tag{3.207}$$

This quantization condition thus states that the k-space area A_n is quantized in the presence of a magnetic field.

Maslov's index appearing in Eq. (3.207) can be found by applying the WKB approximation, as done by [10], on a quantum well with sloping sides. Choosing cutoffs at the turning points x_1 and x_2, such $x_1 < x < x_2$, the WKB wave function can be written either as

$$\psi(x) \approx \frac{2D}{\sqrt{p(x)}}\sin\theta_2(x), \qquad \theta_2(x) \equiv \frac{1}{\hbar}\int_x^{x_2}\mathrm{d}x'\,p(x') + \frac{\pi}{4}, \tag{3.208}$$

or as

$$\psi(x) \approx -\frac{2D'}{\sqrt{p(x)}}\sin\theta_1(x), \qquad \theta_1(x) \equiv -\frac{1}{\hbar}\int_{x_1}^{x}\mathrm{d}x'\,p(x') - \frac{\pi}{4}, \tag{3.209}$$

since the sine function is an odd function. Here p is the momentum of an electron with the energy E and V is the confining potential. Clearly, the phases of the sine functions must be identical modulus π,

$$\theta_2 = \theta_1 + n'\pi, \qquad n' = 1, 2, 3, \ldots \tag{3.210}$$

which yields the Bohr–Sommerfeld quantization rule,

$$\int_{x_1}^{x_2}\mathrm{d}x\,p(x) = \pi\hbar\left(n+\frac{1}{2}\right), \qquad n = 0, 1, 2, \ldots \tag{3.211}$$

By comparing this with Eq. (3.198)—neglecting Berry's phase—we obtain Maslov's index for an electron,

$$\nu = \frac{1}{2}. \tag{3.212}$$

3.6.2 Quantization of Dirac spectrum in magnetic field

As seen in Sec. 3.4, immersing electrons in a magnetic field will force them to move in cyclotron orbits. The area of a cyclotron orbit in k space of a Dirac electron in the low-energy regime is

$$A(k) = \int_0^{2\pi}\mathrm{d}\theta\int_0^{k}\mathrm{d}k'\,k' = \pi k^2, \tag{3.213}$$

and the dispersion relation is $E_\pm(k) = \varepsilon_\mathrm{D} \pm \hbar v_\mathrm{F} k$, so the above equation becomes

$$A(k) = \pi\frac{(E_\pm(k)-\varepsilon_\mathrm{D})^2}{(\hbar v_\mathrm{F})^2}. \tag{3.214}$$

The Onsager quantization rule then dictates that the k-space area is quantized through the index n according to Eq. (3.207), so the energy becomes

$$E_n = \varepsilon_\mathrm{D} \pm \sqrt{2e\hbar v_\mathrm{F}^2 B\left(n+\nu-\frac{\gamma_\mathrm{B}}{2\pi}\right)}. \tag{3.215}$$

In general, the contributions from Maslov's index and Berry's phase will shift the Landau levels. But for a Dirac electron experiencing negligible Zeeman splitting this is de facto not the case. Maslov's index for an electron is $\nu = 1/2$ from Eq. (3.212), and in view of Eq. (3.183), a Dirac electron acquires

a Berry phase of $\gamma_{\mathrm{B}} = \pi$ (here we are only interested in the *magnitude* of Berry's phase) when the Zeeman energy is negligible. Hence Maslov's index and Berry's phase cancel each other, such that

$$\nu - \frac{1}{2\pi}\gamma_{\mathrm{B}} = 0, \tag{3.216}$$

and Eq. (3.215) simplifies to

$$E_n = \varepsilon_{\mathrm{D}} \pm \sqrt{2eB\hbar v_{\mathrm{F}}^2 n}. \tag{3.217}$$

This is the same result as was obtained in the ladder-operator approach in Eq. (2.46) with no Zeeman-energy contribution. Actually, what we did was just to quantize the wave number k into something depending on the magnetic field and the level index n *pretending that the Zeeman effect had no influence on the wave number*. This is clearly realized by equating the energy in Eq. (3.217) to the nonquantized low-energy dispersion relation,

$$\varepsilon_{\mathrm{D}} \pm \sqrt{2eB\hbar v_{\mathrm{F}}^2 n} = E_n = \varepsilon_{k_n} = \varepsilon_{\mathrm{D}} \pm \hbar v_{\mathrm{F}} k_n, \tag{3.218}$$

yielding a quantization condition on the wave number

$$k_n = \sqrt{\frac{2eB}{\hbar} n} = \frac{\sqrt{2}}{l_B}\sqrt{n}. \tag{3.219}$$

Inserting this result for k_n into

$$E_{n,\pm} = \varepsilon_{\mathrm{D}} \pm \sqrt{\varepsilon_{\mathrm{Z}}^2 + (\hbar v_{\mathrm{F}} k_n)^2}, \tag{3.220}$$

we actually obtain the *exact* result as in Eq. (2.46).

In cases where the trick of quantizing the wave number is inapplicable, one can instead utilize Eq. (3.215) directly, upon using Eq. (3.183),

$$\nu - \frac{1}{2\pi}\gamma_{\pm} = \frac{1}{2} - \frac{1}{2\pi}\left|\mp\pi\left(1 - \frac{\varepsilon_{\mathrm{Z}}}{\sqrt{\varepsilon_{\mathrm{Z}}^2 + \varepsilon_\kappa^2}}\right)\right| = \frac{1}{2}\frac{\varepsilon_{\mathrm{Z}}}{\sqrt{\varepsilon_{\mathrm{Z}}^2 + \varepsilon_\kappa^2}}, \tag{3.221}$$

since $0 < {}^{\varepsilon_{\mathrm{Z}}}/_{\sqrt{\varepsilon_{\mathrm{Z}}^2+\varepsilon_\kappa^2}} < 1$. Semiclassically, one thus gets the following energy spectrum

$$E_{n,\pm} = \varepsilon_{\mathrm{D}} \pm \sqrt{2eB\hbar v_{\mathrm{F}}^2 \left(n + \frac{1}{2}\frac{\varepsilon_{\mathrm{Z}}}{E_{n,\pm} - \varepsilon_{\mathrm{D}}}\right)}. \tag{3.222}$$

Solving for the energy $E_{n,\pm}$ and plotting it as a function of the magnetic field strength in this gives the result in Fig. 3.11 for the first four Landau levels above the zero mode (i.e. $n = 1, 2, 3, 4$) along with the exact result Eq. (2.46). A perfect match between these two energy spectra is seen in the low-field limit. As the magnetic field strength reaches (unrealistic) high field strengths the two dispersions begin to separate as seen in Fig. 3.12. As seen the separation is more pronounced for low-lying levels than for higher-lying levels.

3.6.3 Quantization with warping

When warping effects are included in the description of the electron system, the constant-energy contour is no longer circular but rather warped into a hexagonally-shaped isoenergy surface. The area of this surface for a given energy E can be divided up into 12 part with equal area where one slice is traced out by $\mathbf{k}(\theta, E)$ from 0 to $\pi/6$. The k-space area is now

$$A_n = 12\int_0^{\pi/6} \mathrm{d}\theta \int_0^{k(\theta,E)} \mathrm{d}k\, k = 12\int_0^{\pi/6} \mathrm{d}\theta\, \frac{k^2(\theta,E)}{2} = 6\int_0^{\pi/6} \mathrm{d}\theta\, k^2(\theta,E), \tag{3.223}$$

where the θ parametrization of the modulus of the wavevector comes from solving

$$E(k) = \varepsilon_{\mathrm{D}} \pm \sqrt{(\varepsilon_{\mathrm{Z}} + 2\lambda\hbar^3 \cos 3\theta k^3)^2 + (\hbar v_{\mathrm{F}} k)^2} \tag{3.224}$$

for k. This is done numerically. The band energy E as a function of n is then found by solving the equation

$$6\int_0^{\pi/6} \mathrm{d}\theta\, k^2(\theta,E) = 2\pi\frac{eB}{\hbar}\left(n + \nu - \frac{1}{2\pi}\gamma_{\mathrm{B}}\right), \tag{3.225}$$

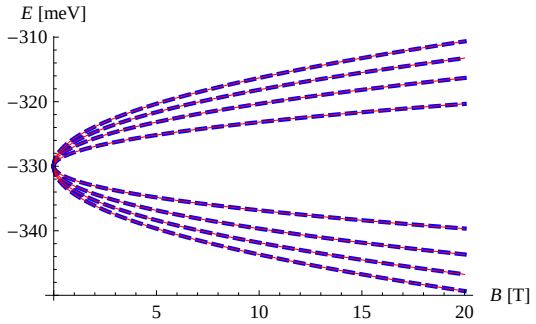

Figure 3.11: Energies for the Landau levels $n = 1, 2, 3, 4$. The Berry-phase modified energy spectrum from Eq. (3.222) (dashed blue line) and the eigenenergies from Eq. (2.46) (red line).

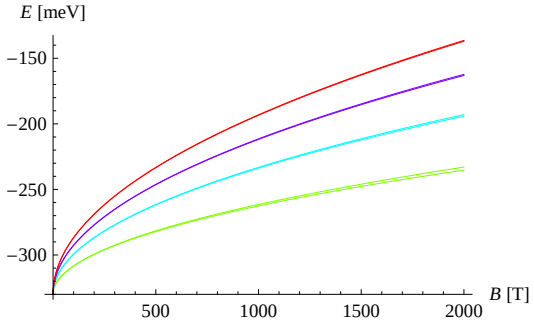

Figure 3.12: Each color pair consists of a Berry-phase modified energy from Eq. (3.222) and the corresponding eigenenergy from Eq. (2.46). As the magnetic field strength is increased, the pair energies begin to separate.

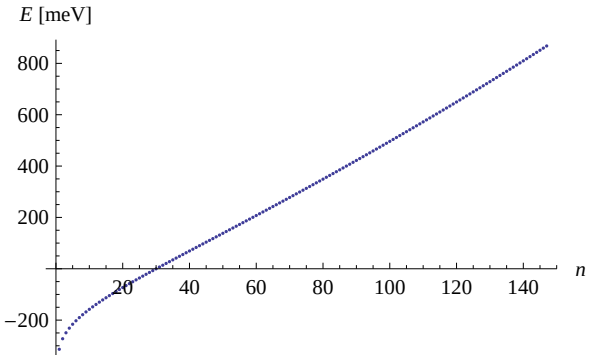

Figure 3.13: Energies from Eq. (3.225).

where the warped Berry phase is given by Eq. (3.86). A plot of the first 145 Landau-level energies is shown in Fig. 3.13. Here it is seen that the energy curve obtains a positive curvature at about $n = 45$, which comes from the warping effect.

We now compare the numerical results of Fig. 2.2 with the semiclassical results in Fig. 3.13. On inspection of Fig. 3.14 the energies from the semiclassical result and the numerical result is seen to be approximately identical. Their difference is seen in Fig. 3.15, from which we notice that the energies of the two models agree fairly well in the low-middle level regime, whereas for higher levels, $n > 90$, the energy discrepancy increases. This could very well be due to finite-size effects of the dimension of the Hamiltonian used in the numerical model.

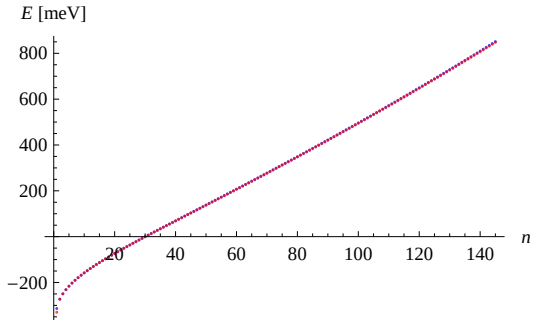

Figure 3.14: Semiclassically (blue curve) and numerically (red curve) eigenenergies for a helical electron with positive helicity.

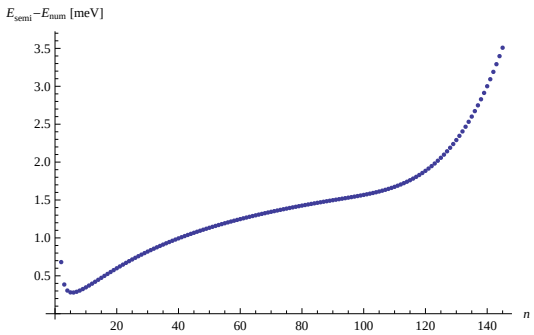

Figure 3.15: Difference in the energies of the semiclassical model and the numerical model.

4 Conclusion and outlook

4.1 Conclusion

In this thesis the nature of the spin–momentum locked surface states which is the hallmark of topological insulators has been investigated. One interesting consequence of this spin–momentum locking effect is that an electron on the surface of a topological insulator will have a Berry phase of π, instead of zero, which is the case for surface-state electrons in a conventional metal. The existence of these special topological-insulator surface-state electrons is guaranteed by the spin–orbit interaction and time-reversal symmetry.

Several properties of a three-dimensional topologically insulating system was investigated. In Ch. 1 it was found that the density of states changes significantly when the warping effect stemming from the underlying crystal-structure anisotropy was included: In the low-energy regime the density of states was linear, but at higher energies the density of states was lower than that expected for low energies.

In Ch. 2 we first utilized quantum-mechanical methods to get insight in the quantum-mechanical behavior of the considered Dirac system. The energy spectrum was found to differ from the well-known energy spectrum for a conventional metal in that it has a $\sqrt{n}$ dependence in vanishing Zeeman field, instead of a n dependence. This special spectrum also gives rise to a zero mode residing exactly at the Dirac-point energy. Including the Zeeman field will induce a gap in the energy spectrum.

Afterwards, the quantized energy spectrum with the warping effect was found using a numerical model. It was found that the warping effect increases (decreases) the energy of a positive- (negative) helicity electron. These results were then used to compute the density of states for an electron on the surface of a topological insulator. Landau levels in the low-energy regime were clearly seen, as was the effect of warping as it shifted the levels towards higher energies. However, the exact effect on the Fermi-surface density of states from the mixing of bulk conduction band-induced surface states and topological surface states are still to be uncovered, since the numerical calculations in this thesis did not bring any clear results on this matter.

In Ch. 3 we investigated how the Dirac electrons in a topological insulator behaved using mainly a semiclassical approach. We first considered a mass-gapped Dirac system, and found that it took a splitting of the energy spectrum to induce nontopological Berry phase, i.e. a Berry phase other than π. As the magnetic field vanished, the topological Berry phase of π was recovered. Next it was found that the warping had an effect on Berry's phase, in such a way that Berry's phase would increase with an increasing warping strength.

After this we investigated one effect of the anomalous velocity, namely the anomalous quantum Hall effect in which a current transverse to the electric field flows. This intrinsic quantum Hall effect comes directly from the Berry-phase supported anomalous velocity appearing in a semiclassical treatment of the wave packet dynamics. The anomalous quantum Hall was later obtained using a many-body Green's function approach, and the Hall conductivity was found to be quantized in units of $(e^2/\hbar)/(4\pi)$.

We used semiclassical quantization rules to quantize the classically found energy spectrum. It was shown that the energy spectrum of a Dirac electron in a magnetic field could be obtained exactly by a semiclassical quantization procedure. Forging on, the eigenenergies with warping was found numerically using hte Bohr–Sommerfeld quantization condition together with the warped Berry phase, and the eigenenergies were seen to be in good agreement with the eigenenergies found by a numerical model in which the Hilbert space approximated to be finite.

4.2 Outlook

4.2.1 Warped Berry phase in magnetic field

Even though it shown that the warping effect changed Berry's phase, it was only done for a *mass*-gapped system, and not, as preferable, for a *magnetically* gapped system. A technical obstacle is that a magnetic field couples the real-space dynamics with the momentum-space dynamics, through the canonical momentum with its dependence on the chosen gauge, e.g. a symmetric gauge, $\mathbf{A} = \mathbf{B} \times \mathbf{r}/2$. One then has to solve Hamilton's equations in order to find the the position $\mathbf{r}$ and the momentum $\mathbf{r}$. This was done, but the resulting Berry phase was unphysical (complex), and some new ideas are hereby needed.

4.2.2 Effect of anomalous velocity on the cyclotron orbits

The cyclotron orbits in Sec. 3.4 were derived from the Rashba Hamiltonian and the result was rather trivial, namely circular orbits, as in the case of conventional metals (although the frequency was different). But in Sec. 3.1 it was shown that, in general, an anomalous velocity has to be included to describe the dynamics of the system. The anomalous velocity will change Hamilton's equation Eq. (3.131), such that

$$\dot{\mathbf{r}} = \frac{1}{\hbar}\frac{\partial E}{\partial \mathbf{k}} - \dot{\mathbf{k}} \times \mathbf{B}_{\mathrm{B}}. \tag{4.1}$$

So anomalous-velocity effect do not appear in the Rashba Hamiltonian itself, but rather in a modified version of Hamilton's equations. Including this effect could change the cyclotron orbits.

4.2.3 Extra velocity from the orbital magnetic moment of the wave packet

It would be interesting to see what effect the extra velocity arising from the orbital magnetic moment—coming from the $\mathbf{B} \cdot \mathbf{L}$ term in Eq. (3.32)—of the wave packet has on the dynamics of the topological surface-state electrons. The term does contain Berry's connection, so this is apparently also a Berry-phase supported velocity.

A Appendix

A.1 Scattering on a localized nonmagnetic impurity potential

We consider an electronic state $|\mathbf{k},\eta\rangle$ which scatters on a fixed nonmagnetic impurity with impurity density $n_{\mathrm{imp}} = {}^{N_{\mathrm{imp}}}\!/_{\mathcal{A}}$ residing on a two-dimensional surface, $\mathcal{A}$ being the area of the sample. The electronic state is scattered to the state $|\mathbf{k}',\eta'\rangle$ through the scattering angle,

$$\theta_{\mathbf{k}\mathbf{k}'} \equiv \phi_{\mathbf{k}'} - \phi_{\mathbf{k}}. \tag{A.1}$$

An electronic state with helicity η can can be represented by

$$|\mathbf{k},\eta\rangle = |\mathbf{k}\rangle \otimes (|\uparrow\rangle + \eta\, \mathrm{e}^{\mathrm{i}\phi_{\mathbf{k}}}\, |\downarrow\rangle), \tag{A.2}$$

with the normalized plane-wave electronic states being represented by

$$|\mathbf{k}\rangle = \frac{1}{\sqrt{\mathcal{A}}}\, \mathrm{e}^{\mathrm{i}\mathbf{k}\cdot\mathbf{r}} \tag{A.3}$$

and we get

$$\begin{aligned}\langle \mathbf{k}',\eta'|U_{\mathrm{imp}}|\mathbf{k},\eta\rangle &= \big(\langle\uparrow| - \eta'\, \mathrm{e}^{-\mathrm{i}\phi_{\mathbf{k}'}}\, \langle\downarrow|\big) \otimes \langle \mathbf{k}'|U_{\mathrm{imp}}|\mathbf{k}\rangle \otimes \big(|\uparrow\rangle + \eta\, \mathrm{e}^{\mathrm{i}\phi_{\mathbf{k}}}\, |\downarrow\rangle\big) \\ &= \langle \mathbf{k}'|U_{\mathrm{imp}}|\mathbf{k}\rangle + \langle \mathbf{k}'|\eta\eta' U_{\mathrm{imp}}\, \mathrm{e}^{\mathrm{i}(\phi_{\mathbf{k}} - \phi_{\mathbf{k}'})}\, |\mathbf{k}\rangle. \end{aligned} \tag{A.4}$$

We assume long-wavelength limit $\lambda \gg a$ or $k \ll 1/a$, where a is the lattice constant (distance between atoms). In this limit we can approximate the impurity potential by a contact potential

$$U_{\mathrm{imp}}(\mathbf{r}) = U_0 \delta(\mathbf{r}), \tag{A.5}$$

and we simply get the scattering matrix element

$$\begin{aligned}\langle \mathbf{k}'|U_{\mathrm{imp}}|\mathbf{k}\rangle &= \int \mathrm{d}\mathbf{r}\, \frac{1}{\sqrt{\mathcal{A}}}\, \mathrm{e}^{-\mathrm{i}\mathbf{k}'\cdot\mathbf{r}}\, U_0 \delta(\mathbf{r}) \frac{1}{\sqrt{\mathcal{A}}}\, \mathrm{e}^{\mathrm{i}\mathbf{k}\cdot\mathbf{r}} \\ &= \frac{U_0}{\mathcal{A}} \int \mathrm{d}\mathbf{r}\; \mathrm{e}^{\mathrm{i}(\mathbf{k}-\mathbf{k}')\cdot\mathbf{r}}\, \delta(\mathbf{r}) \\ &= U_0. \end{aligned} \tag{A.6}$$

With this Eq. (A.4) becomes

$$|\langle \mathbf{k}',\eta'|U_{\mathrm{imp}}|\mathbf{k},\eta\rangle|^2 = 2U_0^2\big(1 + \eta\eta' \cos\theta_{\mathbf{k}\mathbf{k}'}\big). \tag{A.7}$$

A.2 Orbital magnetic moment of electron wave packets

The $\mathbf{B} \cdot \mathbf{L}$ term as given by Eq. (3.32) from [12] gives rise to an extra velocity contribution to the electron wave packet,

$$\dot{\mathbf{r}}_{\mathrm{m}} = \frac{e}{2m\hbar} B_i \partial_{\mathbf{k}} L_i, \tag{A.8}$$

stemming from the Zeeman-like coupling of the orbital magnetic moment of the wave packet,

$$\mathbf{m}(\mathbf{k}) = \frac{e}{2m} \mathbf{L} \tag{A.9}$$

with the magnetic field $\mathbf{B}$. This is discussed in greater detail in [15], where it is noted that the wave packet of a Bloch electron will rotate around its center of mass and it therefore obtains a orbital magnetic moment. This effect is also discussed in [13].

A.3 Eigenspinors in gapped system

In general, a matrix on the form

$$M = \begin{pmatrix} a_{11} & t \\ t^* & a_{22} \end{pmatrix}, \tag{A.10}$$

has eigenvalues

$$E_\pm = \frac{1}{2}\left(a_{11} + a_{22} \pm \sqrt{(a_{11} - a_{22})^2 + 4|t|^2}\right), \tag{A.11}$$

and normalized eigenvectors

$$\chi_\pm = \frac{1}{\sqrt{2}} \begin{pmatrix} u_\pm \, \mathrm{e}^{\mathrm{i}\theta} \\ \pm u_\mp \end{pmatrix}, \tag{A.12}$$

where

$$u_\pm \equiv \sqrt{1 \pm \frac{a_{11} - a_{22}}{\sqrt{(a_{11} - a_{22})^2 + 4|t|^2}}}, \tag{A.13}$$

$$\theta \equiv \arg t. \tag{A.14}$$

A.4 Cyclotron motion with warping

The *Mathematica* codes which were used to obtain the warped cyclotron motion is

```
ksol = NDSolve[
      Join[
       Table[
        D[p[[i]][t], t] == ((Mmat.Table[D[HamFct[E0, x, y, kx, ky, B, λ], p[[j]]], {j, 4}])[[
             i]] /. {x → x[t], y → y[t], kx → kx[t], ky → ky[t]}), {i, 4}
       ], {x[0] == x0, y[0] == y0, kx[0] == kx0, ky[0] == ky0}
      ],
      {x, y, kx, ky}, {t, 0, 10}
     ][[1]] // Quiet;
```

A.5 Warped eigenenergies in numerical model

The *Mathematica* codes which were used to generate the eigenenergies are given below. The ladder operators were quantized according to

```
null = Table[0, {m, 0, nn, 1}, {n, 0, nn, 1}];
one = IdentityMatrix[nn + 1];
a = Table[If[n == 0, 0, If[m == n - 1, Sqrt[n], 0]], {m, 0, nn, 1}, {n, 0, nn, 1}] // N;
adag = Table[If[m - 1 == n, Sqrt[n + 1], 0], {m, 0, nn, 1}, {n, 0, nn, 1}] // N;
w = (a.a.a + adag.adag.adag);
```

The surface-state and bulk-state Hamiltonians were then defined according to

$$\texttt{Hams[B\_] := }\left\{\left\{\left(\texttt{E0} + \frac{\mu}{2}\,\texttt{gs B}\right)\texttt{one} + \lambda\left(\sqrt{\frac{2\,\texttt{e B}}{\hbar}}\right)^{3}\texttt{w},\ \texttt{i}\sqrt{2\,\hbar\,\texttt{e B}}\ \texttt{v a}\right\},\right.$$

$$\left.\left\{-\texttt{i}\sqrt{2\,\hbar\,\texttt{e B}}\ \texttt{v adag},\ \left(\texttt{E0} - \frac{\mu}{2}\,\texttt{gs B}\right)\texttt{one} - \lambda\left(\sqrt{\frac{2\,\texttt{e B}}{\hbar}}\right)^{3}\texttt{w}\right\}\right\}\ \texttt{// ArrayFlatten}$$

```
Ens[B_] := Ens[B] = Eigenvalues[Hams[B] // N] // Sort;
```

$$\texttt{Hamb[B\_] := }\left\{\left\{\frac{2\,\texttt{e B}}{\hbar}\,\gamma\,\texttt{adag.a} + \left(\gamma\texttt{0} + \frac{\texttt{e B}}{\hbar}\,\gamma + \frac{\mu}{2}\,\texttt{gb B}\right)\texttt{one},\ \texttt{i}\sqrt{\frac{2\,\texttt{e B}}{\hbar}}\ \alpha\,\texttt{a}\right\},\right.$$

$$\left.\left\{-\texttt{i}\sqrt{\frac{2\,\texttt{e B}}{\hbar}}\ \alpha\,\texttt{adag},\ \frac{2\,\texttt{e B}}{\hbar}\,\gamma\,\texttt{adag.a} + \left(\gamma\texttt{0} + \frac{\texttt{e B}}{\hbar}\,\gamma - \frac{\mu}{2}\,\texttt{gb B}\right)\texttt{one}\right\}\right\}\ \texttt{// ArrayFlatten}$$

```
Enb[B_] := Enb[B] = Eigenvalues[Hamb[B] // N] // Sort;
```

References

[1] M. Pesin and A. H. MacDonald. Spintronics and pseudospintronics in graphene and topological insulators. *Nat. Mat.*, 11:409–416, 2012.

[2] M. Z. Hasan and C. L. Kane. *Colloquium:* Topological insulators. *Rev. Mod. Phys.*, 82(4):3045–3067, 2010.

[3] C.-X. Liu, X.-L. Qi, H. Zhang, X. Dai, Z. Fang, and S.-C. Zhang. Model Hamiltonian for topological insulators. *Phys. Rev. B*, 82(4):45122, 2010.

[4] L. Fu, C. L. Kane, and E. J. Mele. Topological Insulators in Three Dimensions. *Phys. Rev. Lett.*, 98(10):106803:1–4, 2007.

[5] W.-C. Lee, C. Wu, D. P. Arovas, and S.-C. Zhang. Quasiparticle interference on the surface of the topological insulator Bi_2Te_3. *Phys. Rev. B*, 80(24):245439:1–5, 2009.

[6] S. Souma, K. Kosaka, T. Sato, M. Komatsu, A. Takayama, T. Takahashi, M. Kriener, K. Segawa, and Y. Ando. Direct Measurement of the Out-of-Plane Spin Texture in the Dirac-Cone Surface State of a Topological Insulator. *Phys. Rev. Lett.*, 106(21):216803:1–4, 2011.

[7] H. Zhang, C.-X. Liu, X.-L. Qi, X. Dai, Z. Fang, and S.-C. Zhang. Topological insulators in Bi_2Se_3, Bi_2Te_3 and Sb_2Te_3 with a single Dirac cone on the surface. *Nat. Phys.*, 5(6):438–442, 2009.

[8] T. Hanaguri, K. Igarashi, M. Kawamura, H. Takagi, and T. Sasagawa. Momentum-resolved Landau-level spectroscopy of Dirac surface state in Bi_2Se_3. *Phys. Rev. B*, 82(8):081305:1–4, 2010.

[9] P. D. C King, R. C. Hatch, M. Bianchi, R. Ovsyannikov, C. Lupulescu, G. Landolt, B. Slomski, J. H. Dil, D. Guan, J. L. Mi, E. D. L. Rienks, J. Fink, A. Lindblad, S. Svensson, S. Bao, G. Balakrishnan, B. B. Iversen, J. Osterwalder, W. Eberhardt, F. Baumberger, and Ph. Hofmann. Large Tunanble Rashba Spin Splitting of a Two-Dimensional Electron Gas in Bi_2Se_3. *Phys. Rev. Lett.*, 107(9):096802:1–5, 2011.

[10] D. J. Griffiths. *Introduction to Quantum Mechanics*. Pearson Prentice Hall, second edition, 2005.

[11] N. A. Sinitsyn. Semiclassical theories of the anomalous Hall effect. *J. Phys. Condens. Matter*, 20(023201):1–17, 2008.

[12] M. Marder. *Condensed Matter Physics*. Wiley, first edition, 2000. Corrected printing.

[13] G. Sundaram and Q. Niu. Wave-packet dynamics in slowly perturbed crystals: Gradient corrections and Berry-phase effects. *Phys. Rev. B*, 59(23):14915–14925, 1999.

[14] G. P. Mikitik and Y. V. Sharlai. The Berry phase in graphene and graphite multilayers. *Low Temp. Phys.*, 34:794–800, 2008.

[15] D. Xiao, M.-C. Chang, and Q. Niu. Berry phase effects on electronic properties. *Rev. Mod. Phys.*, 82(3):1959–2007, 2010.

[16] J. N. Fuchs, F. Piéchon, M. O. Goerbig, and G. Montambaux. Topological Berry phase and semiclassical quantization of cyclotron orbits for two dimensional electrons in coupled band models. *Eur. Phys. J. B*, 77(3):351–362, 2010.

[17] X.-L. Qi, Y.-S. Wu, and S.-C. Zhang. Topological quantization of the spin Hall effect in two-dimensional paramagnetic semiconductors. *Phys. Rev. B*, 74(8):085308:1–7, 2006.

[18] I. M. Lifshitz and A. M. Kosevich. Theory of Magnetic Susceptibility in Metals at Low Temperatures. *Sov. Phys. JETP*, 2(4):636–645, 1956.

[19] A. A. Taskin and Y. Yoichi. Berry phase of nonideal Dirac fermions in topological insulators. *Phys. Rev. B*, 84(3):035301:1–6, 2011.